Oil & Natural Gas Technology

DOE Award No.: DE-NT0006553

Progress Report
First Half 2010

ConocoPhillips Gas Hydrate Production Test

Submitted by:
ConocoPhillips
700 G Street
Anchorage, AK 99501
Principal Investigator: David Schoderbek

Prepared for:
United States Department of Energy
National Energy Technology Laboratory

August 26, 2010

Office of Fossil Energy

Disclaimer

Executive Summary

Accomplishments

- Continued progress toward working interest co-owner approval for proposed production test site
- Further advanced Well Design via Decision & Risk Analysis and Reservoir Simulations

Current Status

- Awaiting Prudhoe Bay Unit working interest owner approval of revised ballot
- Continuing refinement of Well Design logistics and reservoir simulation

Introduction

Work began on the ConocoPhillips Gas Hydrates Production Test (DE-NT0006553) on October 1, 2008. This report is the sixth progress report for the project and summarizes project activities from January 1, 2010 to July 31, 2010. Work during this period was focused on Tasks 3 and 4 from Phase 1 (Site Identification) and Tasks 5 and 6 from Phase 2 (Field Test Planning.)

Task 3 (Phase 1): Field Site Ownership Partner Negotiations

ConocoPhillips continues its efforts to gain permission from Prudhoe Bay Unit co-owners for execution of the production test. ConocoPhillips will continue to keep DOE informed of the progress on gaining formal co-owner approval for the field trial through regular project communications.

Task 4 (Phase 1): Evaluation of Synergies with DOE-BP Arctic Field Project

ConocoPhillips personnel have facilitated meetings with Anchorage-based BP hydrates stakeholders to optimize synergies between the ConocoPhillips CO_2/CH_4 exchange production test and BP's long-term depressurization test. The scenario being evaluated has both tests occurring sequentially from an unused "slot" on the Prudhoe Bay Unit L-pad. The proposal contemplates completion of the COP CO_2/CH_4 exchange test in a near-vertical well. Upon completion of exchange test, perforations will be squeezed,

bridgeplug and whipstock will be set, and the wellbore will be sidetracked for installation of long-term depressurization test. Combination of CO_2/CH_4 exchange field trial and long-term-depressurization project onto a single surface location is under review.

Task 5 (Phase 2): Detailed Well Planning/Engineering

ConocoPhillips performed an extensive in-house engineering peer review and presented results, under the title of Decision and Risk Analysis, to DOE project partners via teleconference on April 8. All design decisions were re-examined and 177 "issues" were sorted into Decisions, Uncertainties, Values/Objectives, and Facts. Three technical and quantifiable objectives of the CO_2/CH_4 exchange project were identified: Carbon dioxide injection, methane production, and sand & water production. Each decision was evaluated relative to its contribution to one or more technical objectives. A wide range of drilling, completion, and stimulation options were evaluated. The three most significant changes to the recommended well plan were elimination of coring, preparations for liquid CO_2/lightweight proppant stimulation, and a 30-day extension of flowback testing.

Task 6 (Phase 2): Pre-Drill Estimation of Reservoir Behavior

ConocoPhillips performed two critical reservoir simulations and developed a 3D geocellular model to perform further simulations during the report period. Results are summarized below and detailed in the following three appendices. Simulations were reviewed with DOE, BP, and ExxonMobil hydrate stakeholders at the Site Selection Workshop held in Denver on May 13. Also in attendance were key USGS personnel (Tim Collett, Warren Agena, Myung Lee, and Chrissy Lewis) and external reservoir simulation experts Brian Anderson (University of West Virginia, Morgantown) and Scott Wilson (Ryder Scott, Denver).

Appendix 1: Heat of Hydration Effects

Author: Suntichai Silpngarmlert, ConocoPhillips Company, Houston, Texas

Summary: Near-wellbore hydrate dissociation caused by heat of cement hydration during casing operations was modeled using TOUGH+Hydrate. In a 8¾" hole, 7" casing can be successfully cemented with LiteCRETE without inducing near-wellbore hydrate dissociation. In washed-out holes, modeling indicates that hydrate dissociation can be minimized by cooling cement to 35 °F.

Appendix 2: Thermal Effects of Hot Fluid Production/Injection in Existing Wells

Author: Suntichai Silpngarmlert, ConocoPhillips Company, Houston, Texas

Summary: Thousands of wells transect the North Slope gas-hydrate stability zone. Nearly all are completed significantly deeper than hydrate-bearing sandstones, and many of these wells produce or inject fluids significantly hotter than hydrate-stability conditions. TOUGH+Hydrate was utilized to simulate the effects of hot fluid production and injection on near-wellbore hydrate stability. Simulation indicates that, although a 1 °F-temperature increase may extend over 125 feet from a producing well, hydrate dissociation is limited to less than 60 feet from an inclined producer. Over the ten-year producing life simulated, modeling indicates that sufficient gravity segregation may occur such that free gas remains stable inside the gas-hydrate stability zone.

Appendix 3: Geocellular Model for Evaluation of Gas Hydrate Production Mechanism in Selected Sandstones of the Sagavanirktok Formation

Author: Mark Scheihing, ConocoPhillips Company, Anchorage, Alaska

Summary: A 3D geocellular model has been constructed utilizing depth-converted 3D seismic and wireline data (mostly gamma-ray logs) for the nine-square-mile area surrounding Prudhoe Bay Unit L-pad. The model integrates ten seismic/subsurface faults and fourteen layers, from Sagavanirktok "F Sandstone" to "B Sandstone." A non-linear grid has been populated with reservoir properties derived from interpretation of Prudhoe Bay Unit L-106 logs and integration of Mt Elbert #1 log and core data.

Cost Status

Expenses incurred during this period were below the Baseline Cost Plan as shown in Exhibit 1.

COST PLAN/STATUS									
Project Phase ==>	Phase 1, Site Ident.		Phase 2, Field Test Planning						
Baseline Reporting Quarter ==>	Q408	Q109	Q209	Q309	Q409	Q110	Q210	Q310	Q410
BASELINE COST PLAN									
Federal Share	0	0	60000	1450000	0	0	0	0	0
Non-Federal Share	325100	499172	390875	333875	170699	0	0	0	0
Total Planned	325100	499172	450875	1783875	170699	0	0	0	0
Cumulative Baseline Cost	325100	824272	1275147	3059022	3229721	3229721	3229721	3229721	3229721
ACTUAL INCURRED COSTS									
Federal Share	0	0	0	0	0	0			
Non-Federal Share	121012	186099	275348	354447	254734	358001	250044		
Total Incurred Cost	121012	186099	275348	354447	254734	358001	250044		
Cumulative Incurred Cost	121012	307111	582459	936906	1191640	1549641	1799685		
VARIANCE									
Federal Share	0	0	-60000	-1450000	0	0	0		
Non-Federal Share	-204088	-313073	-115527	20572	84035	358001	250044		
Total Variance	-204088	-313073	-175527	-1429428	84035	358001	250044		
Cumulative Variance	-204088	-517161	-692688	-2122116	-2038081	-1680080	-1430036		

Exhibit 1: Cost Plan/Status

Milestone Status

The Milestone Status is shown in Exhibit 2 below.

MILESTONE STATUS REPORT						
#	Task/Subtask Description	Planned Start Date	Planned End Date	Actual Start Date	Actual End Date	Comments
	Field trial site selected	1-Oct-08	31-Mar-09	1-Oct-08	3-Apr-09	Top sites identified
	Partner negotiations completed	15-Feb-09	31-Mar-09	17-Mar-09		Ongoing
	Synergies with DOE-BP project identified	1-Mar-09	31-Mar-09	30-Mar-09		Ongoing
	Well test designed and planned	1-Apr-09	30-Sep-09	10-Mar-09		Ongoing
	Well and reservoir performance predicted	1-Jul-09	31-Dec-09	22-Jun-09		Ongoing
	Field testing completed	1-Jan-10	31-Dec-10			
	Injection and production monitoring completed	1-Apr-10	30-Apr-10			
	Well abandonment complete	1-May-10	31-Dec-10			

Exhibit 2: Milestone Status

Appendix 1: Heat of Hydration Effects
Author: Suntichai Silpngarmlert, ConocoPhillips Company, Houston, TX

The effect of heat released by cement hydration during casing operations on the stability of near-wellbore hydrate was modeled in this simulation study. Heat of hydration effects were examined in three different cases (see Figure 1-1). All three cases have the same casing diameter (7"), but they have different hole-diameters: 8-3/4", 16", and 24;" the larger diameters simulate enlarged or washed-out holes. Cold fluid circulation inside the casing, pumped while cement is hydrating, was examined as a potential strategy to mitigate heat of hydration effects for the same three cases; modeled assumption is that inner-string circulation can keep fluid temperature in the wellbore constant at 26°F.

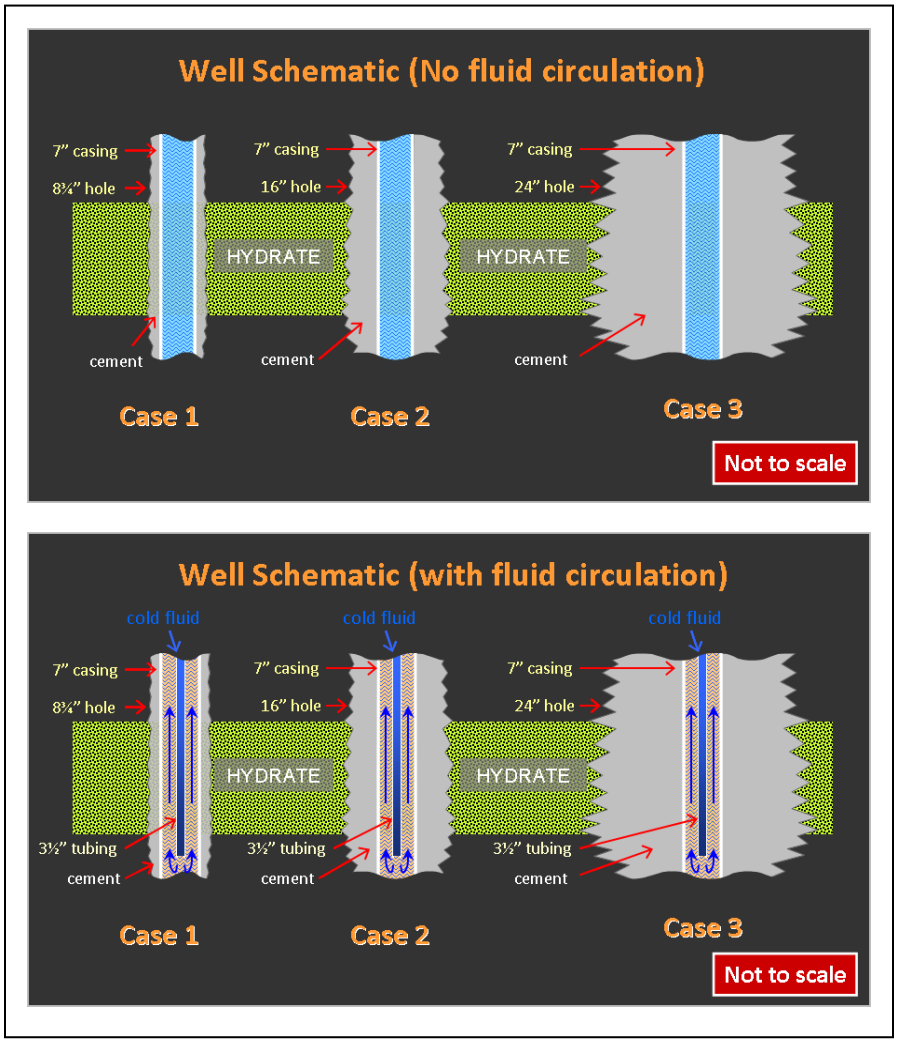

Figure 1-1: Well-schematic of three simulation cases

Heat of hydration of "LiteCRETE" cement, a low heat-of-hydration cement, was modeled in this study. Heat evolution during a cementing job can be divided into 3 stages (see Figure 1-2). Heat generation in stage 1 occurs at the surface during mixing of

cement slurry; and there is no heat generated during stage 2. The heat released in stage 1 increases the temperature of cement slurry at the surface. Heat of hydration effects on near-wellbore hydrate are only caused by heat transfer (from cement slurry to the hydrate) during stages 2 and 3. The heat released during stage 1, therefore, was excluded from this simulation study. The time periods for stages 2 and 3 were assumed to be 4 hours for each stage. In this study, cold fluid circulation started 1 hour prior stage 3. The heat released in stage 3 (for LiteCRETE cement) is 100 MJ/m^3 (at 10.5 lb/gal slurry).

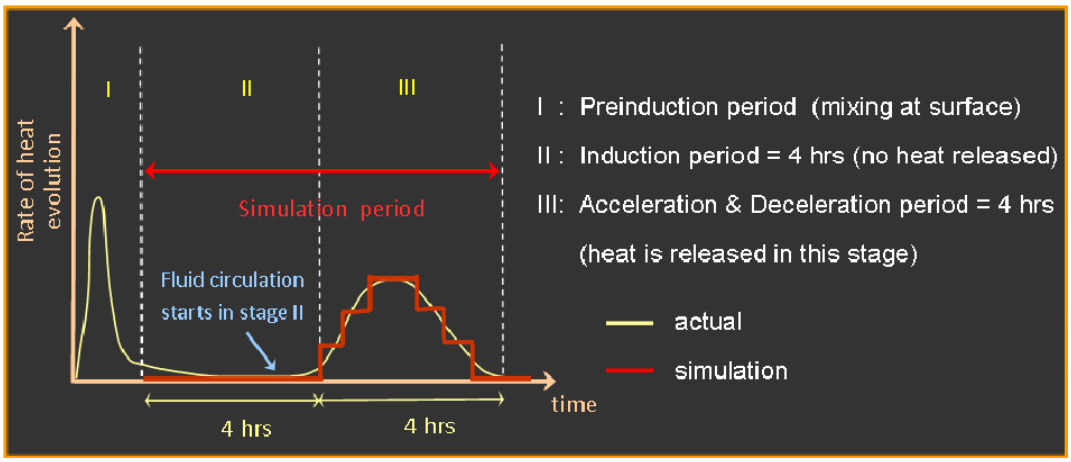

Figure 1-2: Heat of evolution during well-cementation

Simulation model description

A 2-D homogeneous model was built with the following reservoir properties:

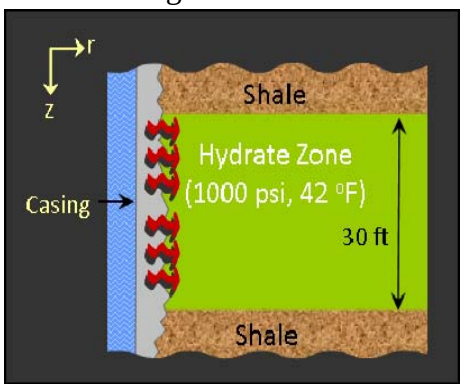

- Initial condition: 1000 psi and 42 °F
- 35% porosity, 70% hydrate saturation
- 0.8% water salinity
- 42.8°F (6°C) slurry temp
- Cement properties:
  - Specific heat: 0.442 BUT/lb-°F
  - Thermal conductivity = 0.35 BTU/hr-ft-°F

It was assumed that the cement slurry is impermeable. Therefore, no released methane gas from hydrate dissociation can migrate into the cement. Also, water migration from the cement slurry to the formation was assumed to be negligible.

Simulation results

Case 1: 7" casing diameter with 8-3/4" hole diameter

Temperature profiles in the center of the hydrate zone during stages 2 and 3 and after stage 3 are shown in Figure 1-3. Since the amount of heat released depends on the thickness of the cement sheath, this case has the lowest heat released. Simulation predicts no hydrate dissociation around the well even in cases without cold fluid circulation in the wellbore, since heat released is not high enough to increase near-wellbore temperature above hydrate dissociation temperature.

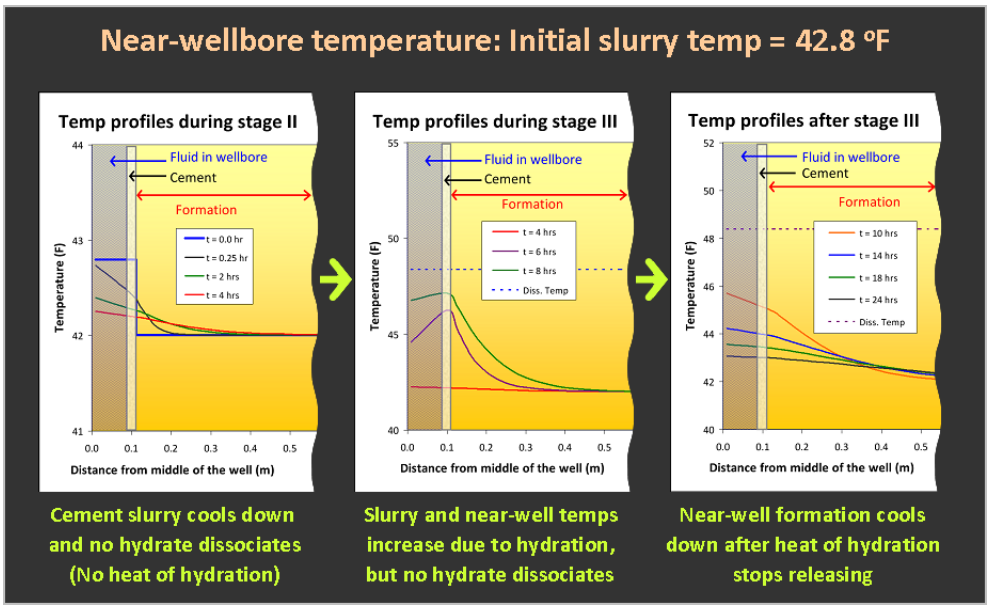

Figure 1-3: Near-wellbore temperature profiles for case 1

Case 2: 7" casing diameter with 16" hole diameter

In this case, modeling predicts dissociation of near-wellbore hydrate even with cold fluid circulation. Fluid circulation inside the wellbore (dashed lines) cannot significantly mitigate near-wellbore heating (middle plot in Figure 1-4). Fluid circulation cools down the near-wellbore formation more rapidly when fluid circulation continues after the end of stage 3. Figure 1-4 shows that fluid circulation (dashed lines) cannot significantly mitigate near wellbore hydrate dissociation, but dissociation is predicted only a few inches from the well.

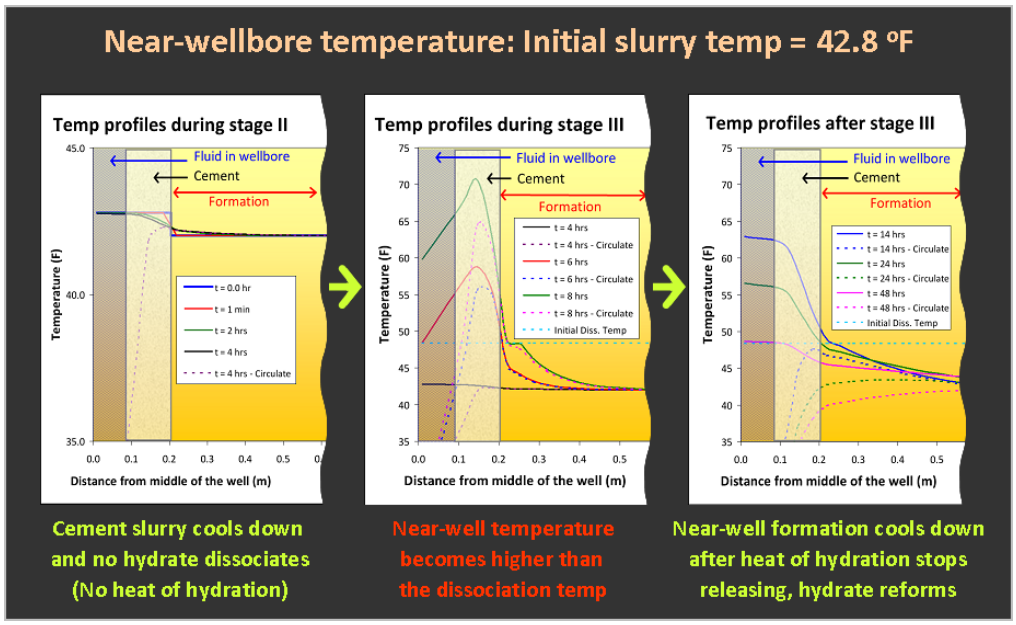

Figure 1-4: Near-wellbore temperature profiles for case 2

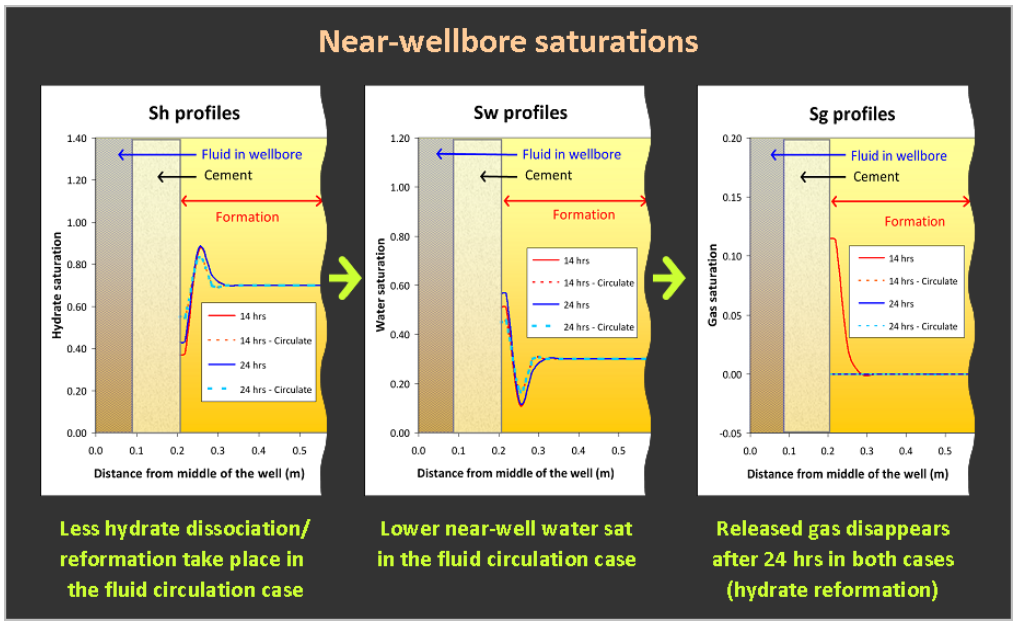

Figure 1-5: Saturation profiles around the well for case 2

Case 3: 7" casing diameter with 24" hole diameter

In this case, modeling also predicts dissociation of near-wellbore hydrate, even with cold fluid circulation. Fluid circulation inside the wellbore (dashed lines) cannot significantly mitigate near-wellbore heating (middle plot in Figure 1-6). The predicted dissociation radius, however, is less than 1 ft from the well.

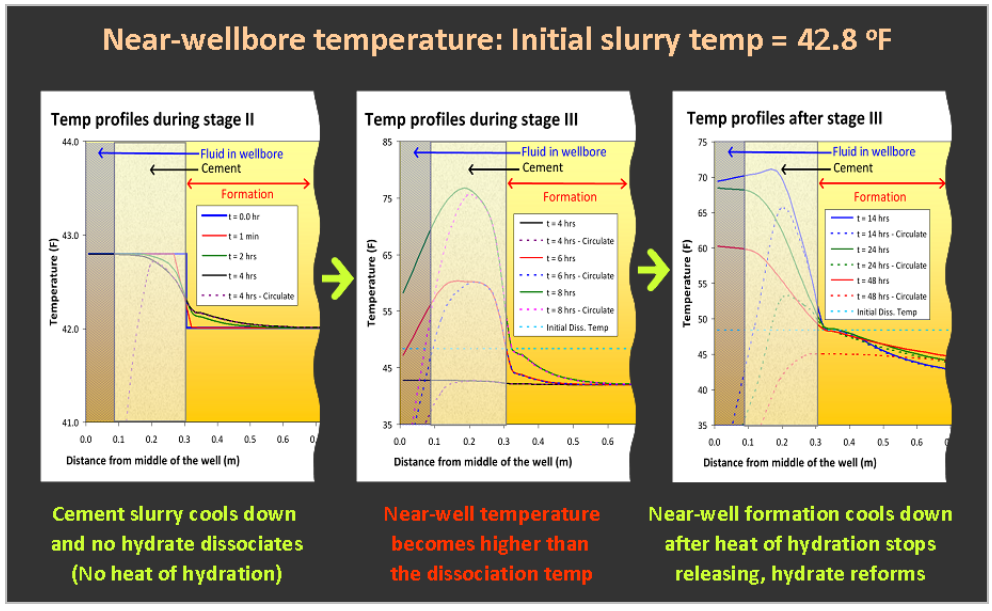

Figure 1-6: Near-wellbore temperature profiles around the well for case 3

Mitigation by lowering cement slurry temperature

Since modeling predicts that cold fluid circulation cannot significantly mitigate near-wellbore hydrate dissociation, mitigation by using colder cement slurry (35 ^{o}F) was also examined. Figure 1-7 compares the temperature profiles between 35 ^{o}F slurry (solid lines) and 42.8 ^{o}F slurry (dashed line) cases. The comparison of saturation profiles around the well of these two cases is shown in Figure 1-8.

A significant decrease of hydrate dissociation is predicted when lowering slurry temperature from 42.8 ^{o}F to 35 ^{o}F.

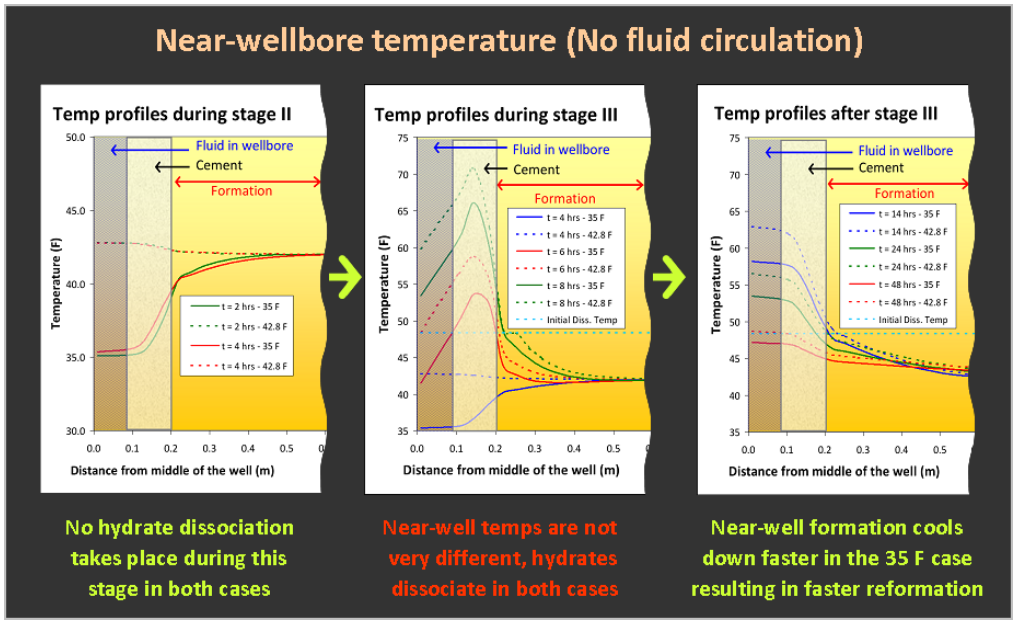

Figure 1-7: Comparison of near-wellbore temperature profiles around the well

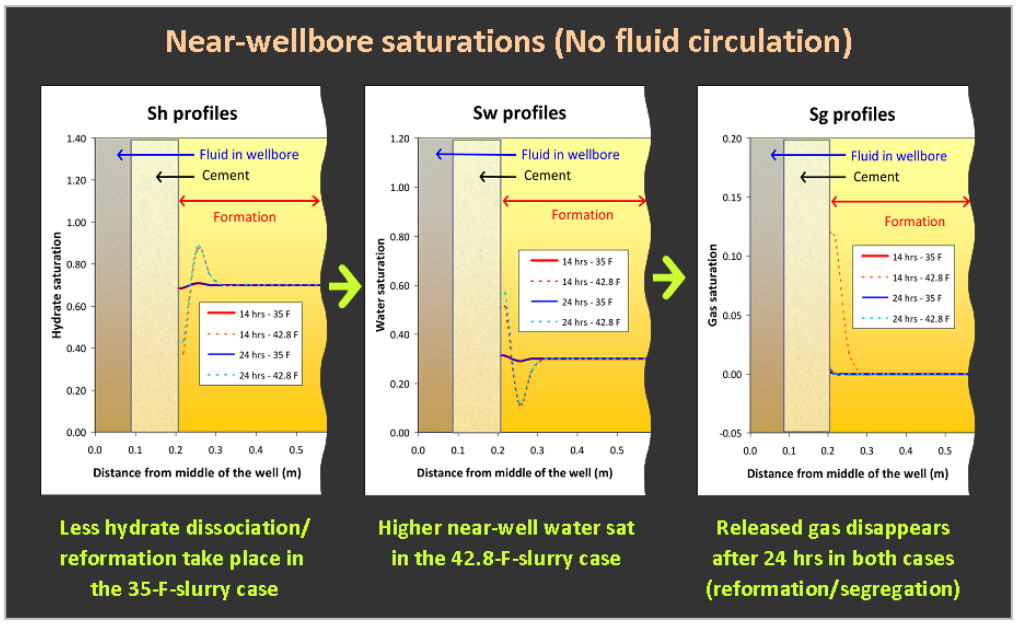

Figure 1-8: Comparison of saturation profiles around the well

Conclusion

The following conclusions can be drawn from this simulation study:

- Near-wellbore hydrate dissociation is not predicted during cementing of 8-3/4" hole.
- Modeling indicates near-wellbore dissociation will occur in a washed-out (16") hole, and cold-fluid circulation does not effectively mitigate dissociation, but dissociation affects a very small radius (few inches from well).
- Hydrate reformation occurs very close to the wellbore. More hydrate dissociation during cement hydration yields higher near-wellbore hydrate saturation (and lower perm) as the system re-equilibrates, challenging injection.
- Lower in-situ formation permeability results in less hydrate dissociation, since near-wellbore pressure increases more rapidly as hydrate dissociates, inhibiting further hydrate dissociation.
- Lowering initial cement slurry temp from 42.8 °F to 35 °F effectively minimizes dissociation of near-wellbore hydrate in the 16" hole case.

Appendix 2: Thermal Effects of Hot Fluid Production/Injection in Existing Wells

The objective of this simulation study is to determine the bottom-hole location of a new well for the pilot test. There are several existing wells around the proposed well. These wells have been producing hot oil/gas from the formation below the hydrate zone. Heat transfer from hot oil/gas in the wellbore can trigger hydrate dissociation around these wells. The estimation of the affected area around these wells needs to be determined before specifying the bottom-hole location of the new well.

2.1 Homogeneous model

Three 2-D homogeneous models representing Prudhoe Bay Unit ("PBU") L-106, L-107, and L-213 were built to simulate production/injection effects on near-wellbore hydrate to determine the affected area from several years of production (L-106 & L-107) and injection (L-213).

2.1.1 PBU L-213

The simplified wellbore schematic of PBU L-213 is shown in Figure 2-1. The temperature of the injected gas was set to be constant at 125 ^{o}F.

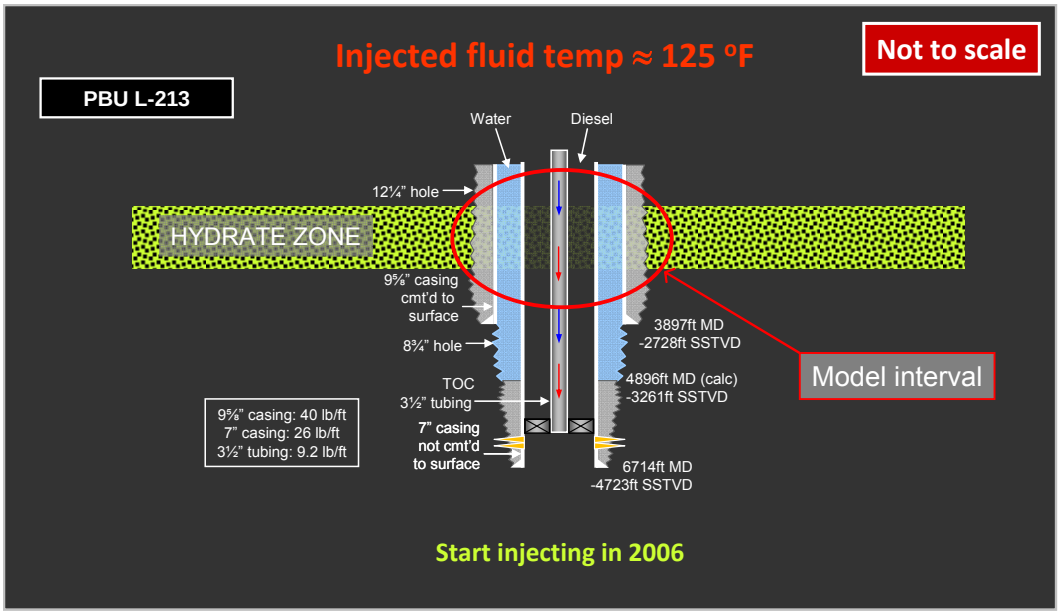

Figure 2-1: Simplified wellbore schematic of PBU L-213

Simulation model description

A 2-D (r-z) homogeneous model was set up with the following reservoir properties:

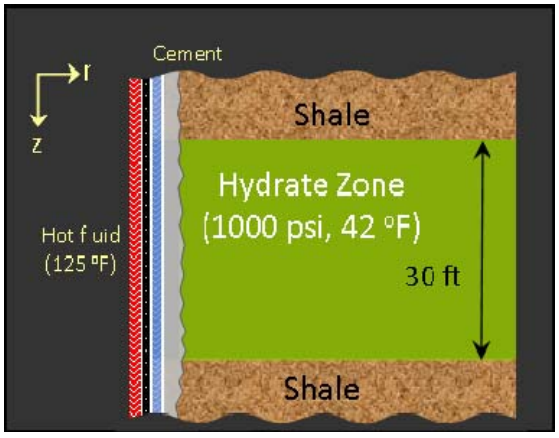

- Initial condition: 1000 psi and 42 ^{o}F
- 35% porosity, 70% SH, 30% Sw
- 0.8% water salinity
- 42.8 ^{o}F (6 ^{o}C) slurry temperature
- Cement properties:
  - Specific heat: 0.442 BUT/lb-^{o}F
  - Thermal conductivity = 0.35 BTU/hr-ft-^{o}F
- Diesel properties:
  - Specific heat: 0.483 BUT/lb-^{o}F
  - Thermal conductivity = 0.39 BTU/hr-ft-^{o}F

Two initial in-situ permeabilities at 70% hydrate saturation (1mD & 5 mD) were simulated.

Simulation results

Figure 2-2 shows the temperature around the well during 3.775 years of injection (the well started operating in late 2006). Temperature profiles of the 1-mD and 5-mD cases are not significantly different. The affected distance is about 80 ft from the well.

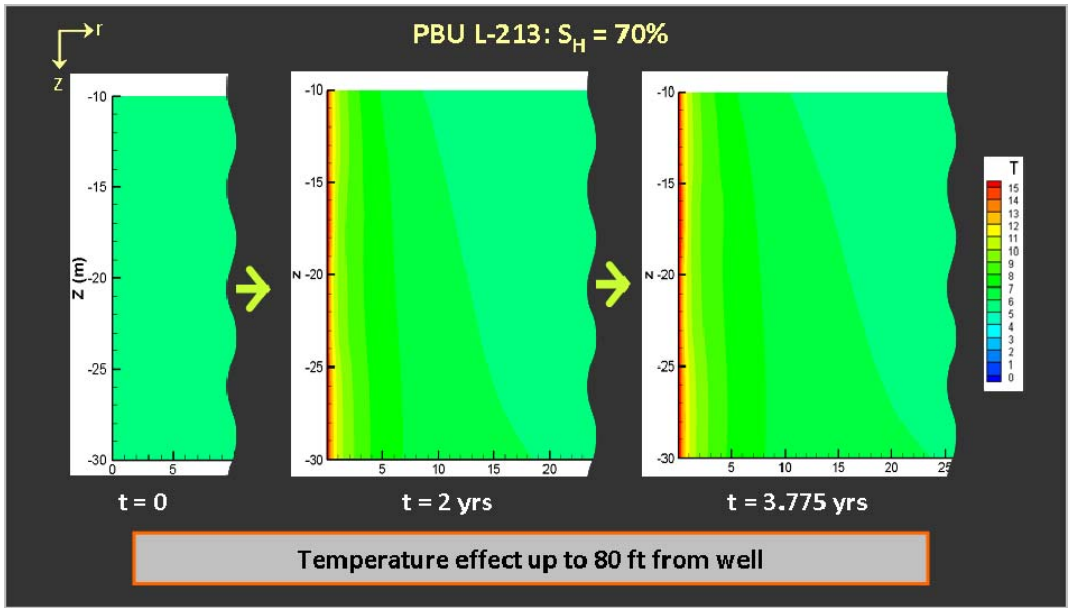

Figure 2-2: Temperature around well L-213 during injection period

Hydrate saturation around the well for the 1-mD and 5-mD cases are significantly different (see Figure 2-3). The model predicts a strongly "banded" structure of low and high hydrate saturation in the 1-mD case. Depressurizaton modeling reported by Moridis and Kowalsky (2006) predicted the formation of alternating bands of high and low hydrate saturation, formed in the direction of fluid flow, as a function of hydrate lensing

caused by capillary pressure effects. In this simulation, bands of alternating high and low hydrate saturation form perpendicular to the wellbore, as methane dissociated from hydrate by heat from the wellbore moves laterally and vertically into regions of lower pressure. The affected distances in the 1-mD and 5-mD cases are 10 ft and 15 ft, respectively.

Figure 2-3 clearly illustrates the effect of permeability on dissociation of near-wellbore hydrate and re-formation in the reservoir as a function of in-situ permeability. Bands of alternating high and low hydrate saturation are not apparent in the 5 mD case. Data from BP - Mt. Elbert #1 indicate that in-situ permeability at 70% hydrate saturation is likely to be less than 1 mD

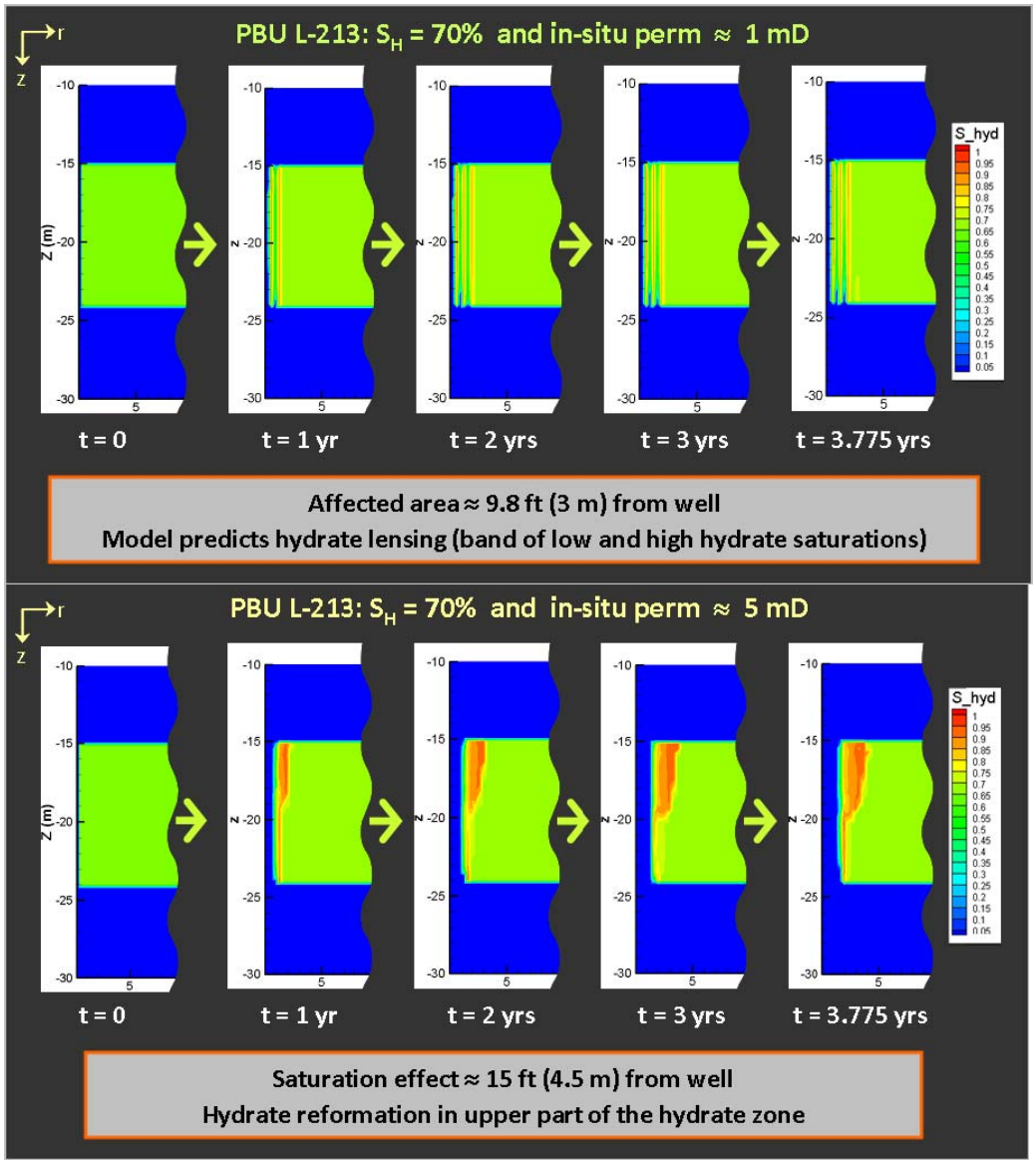

Figure 2-3: Hydrate saturation around well L-213 during the injection period

Similarly, gas saturations around the well for the 1-mD and 5-mD cases are significantly different (see Figure 2-4). The models predict gas accumulation in the upper part of hydrate zone in both cases (due to gravitational effects).

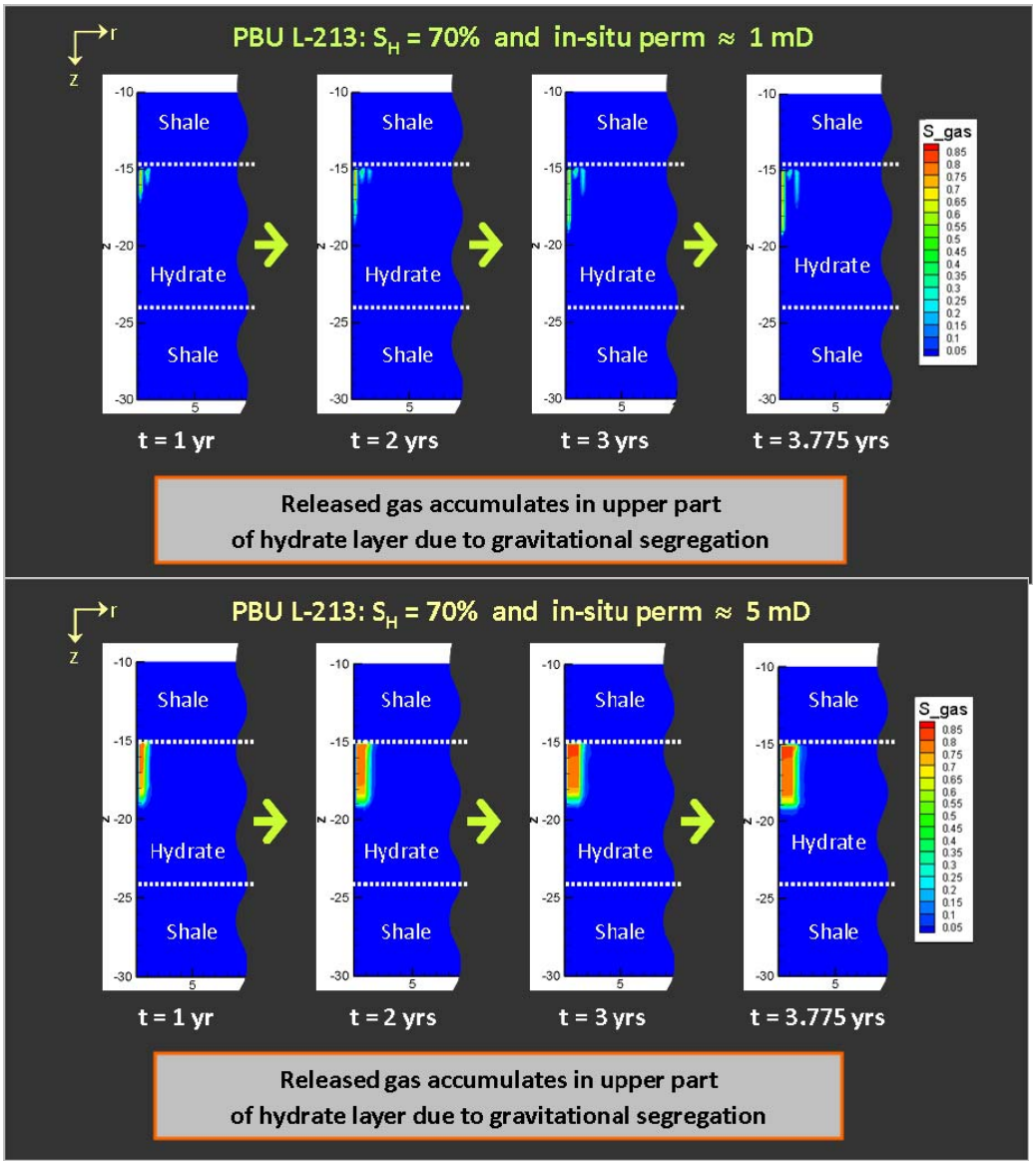

Figure 2-4: Gas saturation around well L-213 during the injection period

2.1.2 PBU L-106 & PBU L-107

Prudhoe Bay Unit L-106 and L-107 are producing wells with similar wellbore configurations. A simplified wellbore schematic of PBU L-106 & L-107 is shown in Figure 2-5. The temperature of the produced fluid, a mixture of oil, gas, and water, was modeled as a constant 125 ^{o}F. Both wells have been operating for about 8.2 years.

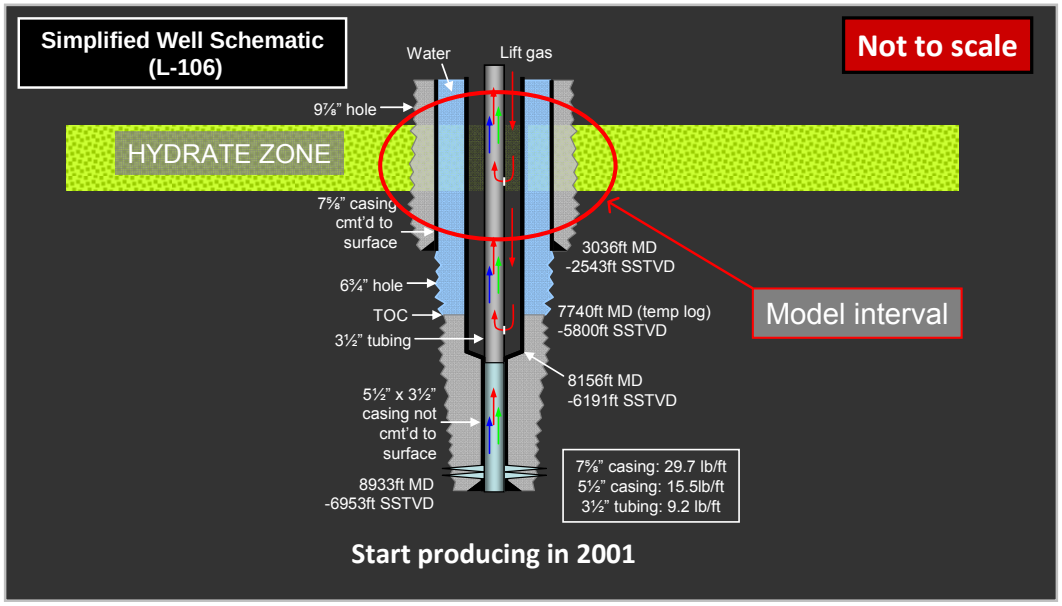

Figure 2-5: Simplified wellbore schematic of PBU L-106 & L-107

Simulation model description

A 2-D homogeneous model was built with the same reservoir properties as those used in the PBU L-213 simulation case. Systems with two different initial in-situ permeabilities at 70% hydrate saturation (1-mD and 5-mD) were simulated.

Simulation Results

Figure 2-6 shows the temperature around the well during 8.2 years of production (the well started operating in late 2001). Temperature profiles of the 1-mD and 5-mD cases are not significantly different. The affected distance is about 115 ft from the well.

Similar to L-213 case, hydrate saturation around the well for the 1-mD and 5-mD cases are significantly different (see Figure 2-7). Modeling predicts a "banded" structure of low and high hydrate saturation in the 1-mD case. The affected distances in the 1-mD and 5-mD cases are 10 ft and 26 ft, respectively.

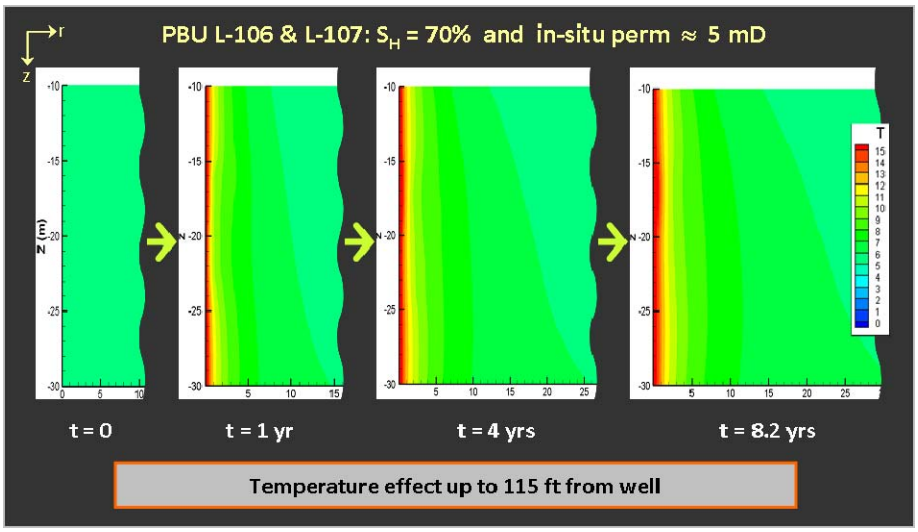

Figure 2-6: Temperature around well during production period

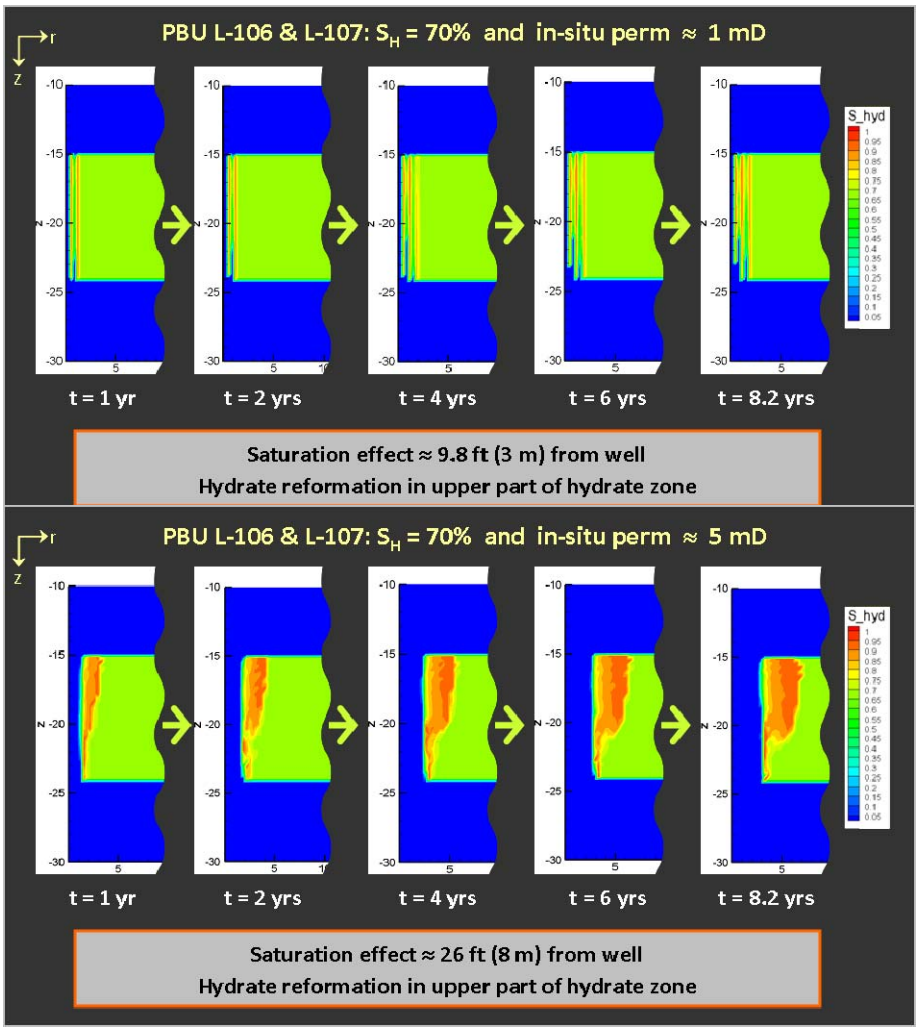

Figure 2-7: Hydrate saturation around well during production period

Gas saturations around the well for the 1-mD and 5-mD cases are also significantly different (see Figure 2-8). Models predict gas accumulation in the upper part of hydrate zone in both cases (due to gravitational segregation effects).

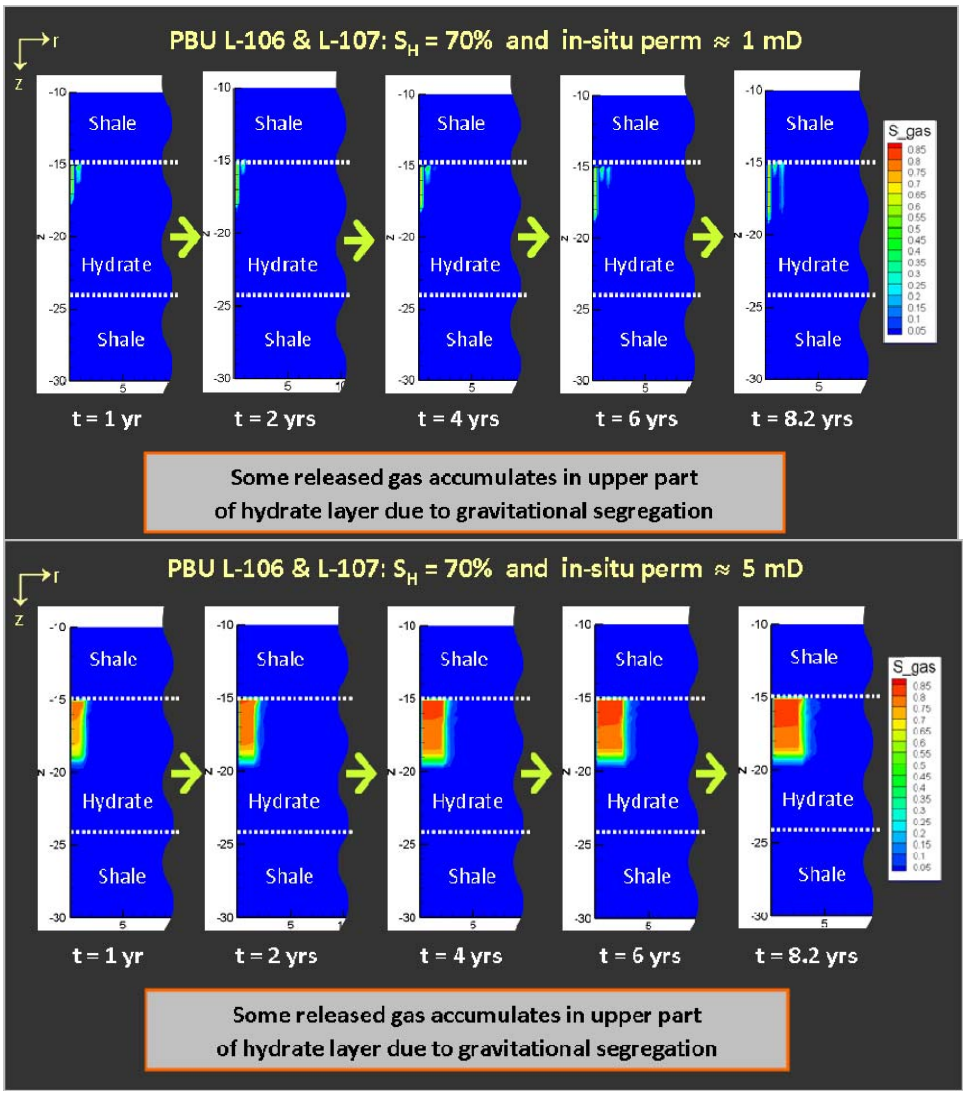

Figure 2-8: Gas saturation around well during production period

Pressures around the well for the 1-mD and 5-mD cases are significantly different (see Figure 2-9). The affected distances in the 1-mD and 5-mD cases are 6 ft and 26 ft, respectively. The models predict very high pressure buildup (pressure increases to about 1750 psi) in the 1-mD case, whereas pressure buildup in the 5-mD case is much lower.

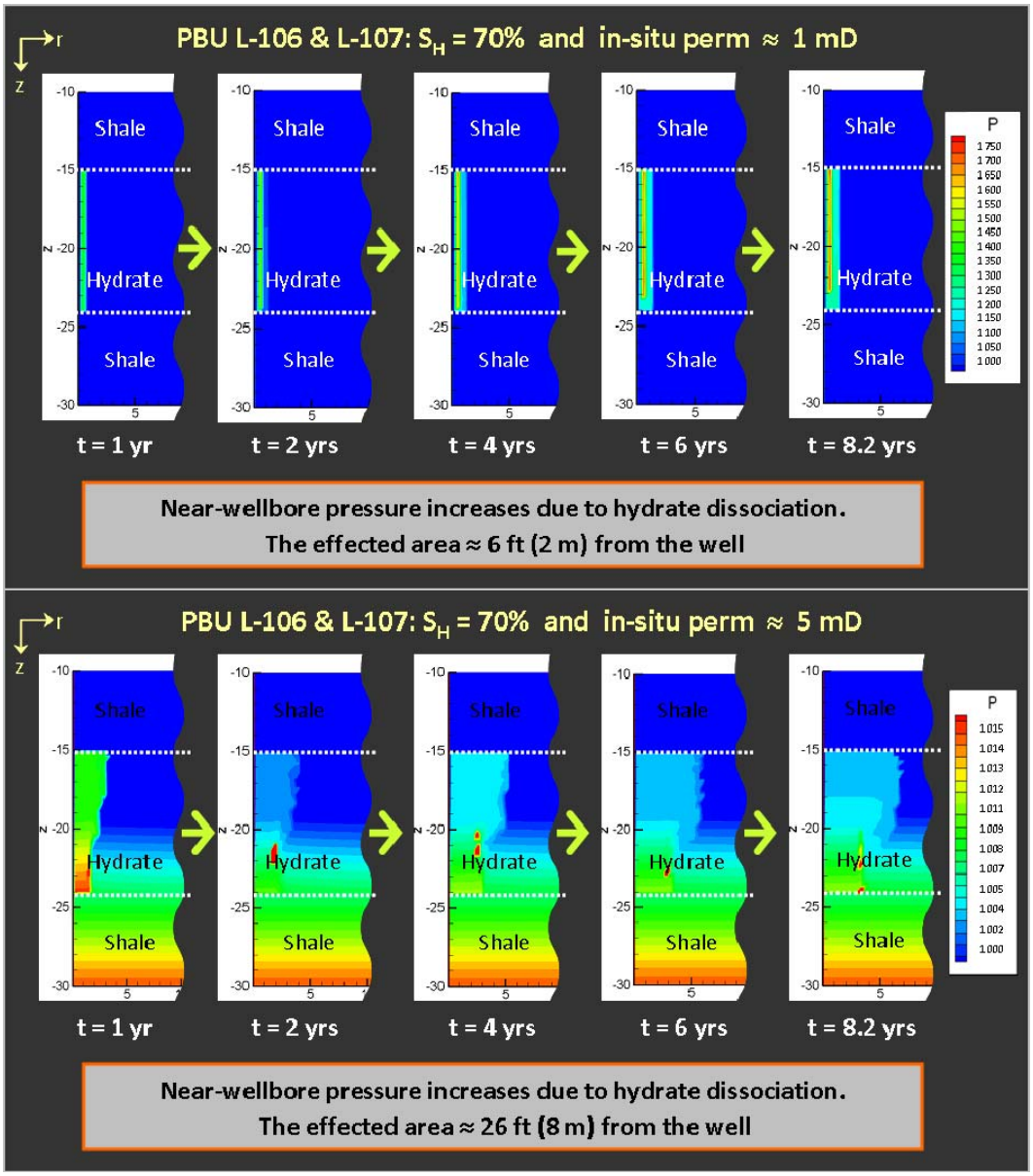

Figure 2-9: Pressure around the well L-106 & L-107 during the injection period

Conclusion

The following conclusions can be drawn from this simulation study of a homogeneous model:

- Heat transfer from the hot fluid in the wells can cause dissociation of near-wellbore hydrates. However, the affected distances around wells L-106, L-107, and L-213 based on hydrate saturation are less than ~26 feet.
- Affected distances around the wells based on temperature profiles are less than ~115 feet from the well.

2.2 Heterogeneous model

In this simulation study, a 2-D model with vertically heterogeneous of porosity and

hydrate saturation (resulting in vertical heterogeneity of in-situ permeability) representing PBU L-106 was built and used to study the effect of hot-fluids production on the stability of near-wellbore hydrates. Figure 2-10 shows log data interpretations from PBU L-106. The S_H curve labeled "from AIM" was used to model vertical stratigraphic variations in hydrate saturation. AIM is an acronym for the Geolog Advanced Interpretation Module. ConocoPhillips has developed an application of this simultaneous equation solver to estimate hydrate saturation from gamma-ray, sonic, density, and neutron-porosity logs. A complete discussion of this approach is reported by Mailloux (2009).

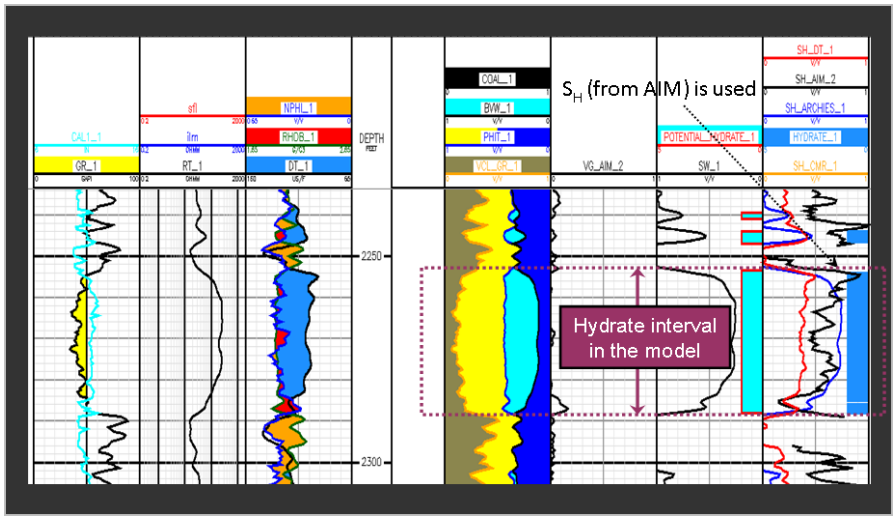

Figure 2-10: PBU L-106 well-log data

Simulation model description

A 2-D model with vertical heterogeneity in porosity and initial hydrate saturation (as described by log-data in Figure 2-10) was used for this simulation study. Model configuration is similar to the configuration utilized in the homogeneous model. In-situ permeabilities, calculated from a built-in correlation in the TOUGH+Hydrate simulator, are consistent with the measured data from Mt. Elbert #1. Initial reservoir conditions are 1000 psi and 42 ^{o}F. In this model, the top seal (above the hydrate zone) is permeable. For this simulation, top-seal permeabilities of 0.1 mD and 1 mD were modeled. Permeability anisotropy (k_v/k_h) for entire model was set at 0.1. Temperature of fluid in the wellbore was modeled at constant 125 ^{o}F. A case with fluid temperature at 165 ^{o}F was also examined as a worst case scenario.

2.2.1 Case 1 ($k_{h\_Top\ seal}$ = 0.1 mD)

In this case, the top seal horizontal vertical permeabilities are 0.1 mD and 0.01 mD, respectively. Calculated in-situ permeability values in hydrate-bearing layer are consistent with measured in-situ permeabilities at Mt. Elbert (0.15 mD at S_H = 75% and 1.5 mD at S_H = 65%).

Simulation Results

Figure 2-11 shows the temperature around the well during 10 years of production. The farthest affected distances in the two cases are not very different (115 ft and 125 ft), but

near-well temperature (within 10 ft around the well) in the 165 ^{o}F case is warmer than that in the 125 ^{o}F case.

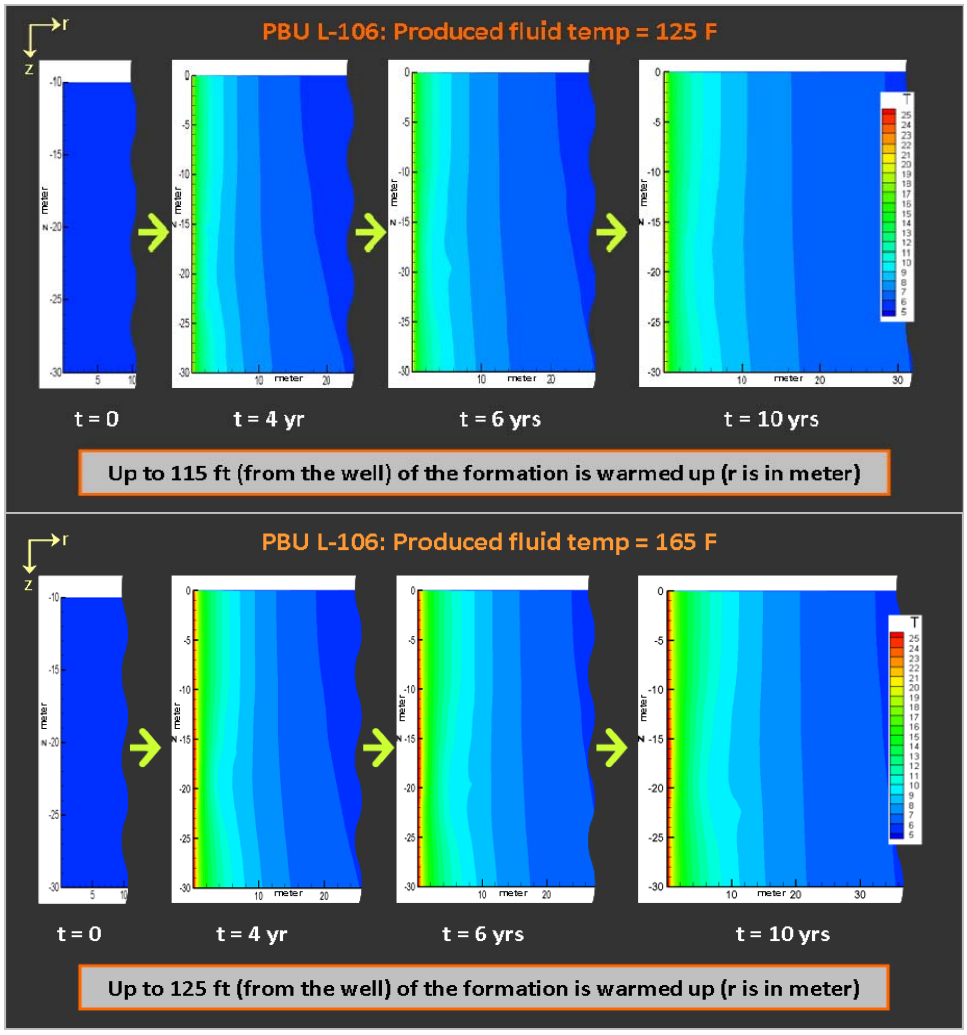

Figure 2-11: Temperature around well during production period

Hydrate saturations around the well for the 125 ^{o}F and 165 ^{o}F cases are significantly different (see Figure 2-12). The affected distances in the 125 ^{o}F and 165 ^{o}F cases are 30 ft and 45 ft, respectively. The model predicts some hydrate formation in the top seal as gas released by hydrate dissociation gas moves into the top seal.

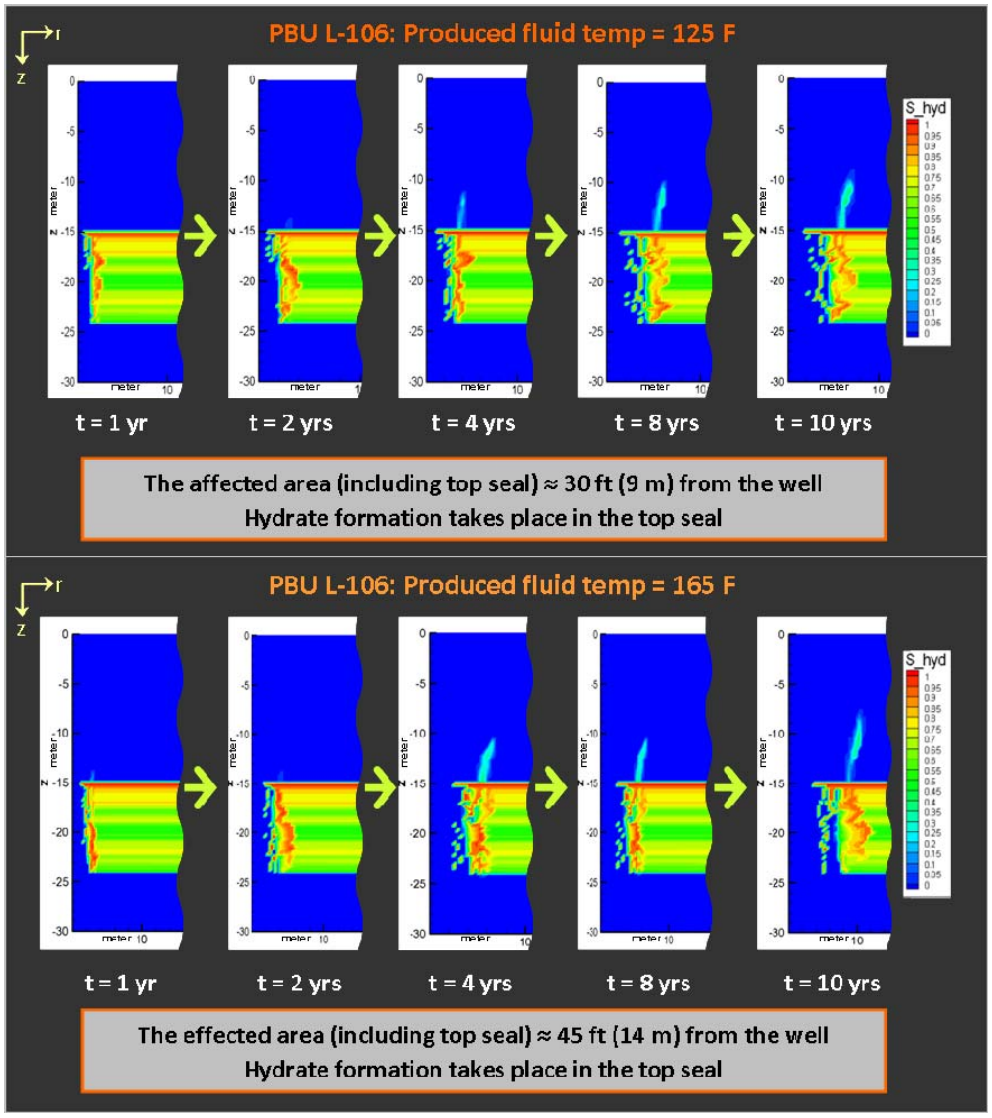

Figure 2-12: Hydrate saturation around well during production period

Gas saturations around the well for the two cases are significantly different (see Figure 2-13) as there is more hydrate dissociation in the 165 ^{o}F producer case. As a result, more gas is released by dissociation in the hydrate-bearing layer and more gas accumulates in the top seal. Released gas is predicted to move into the top seal about 23 ft from the top of the hydrate zone.

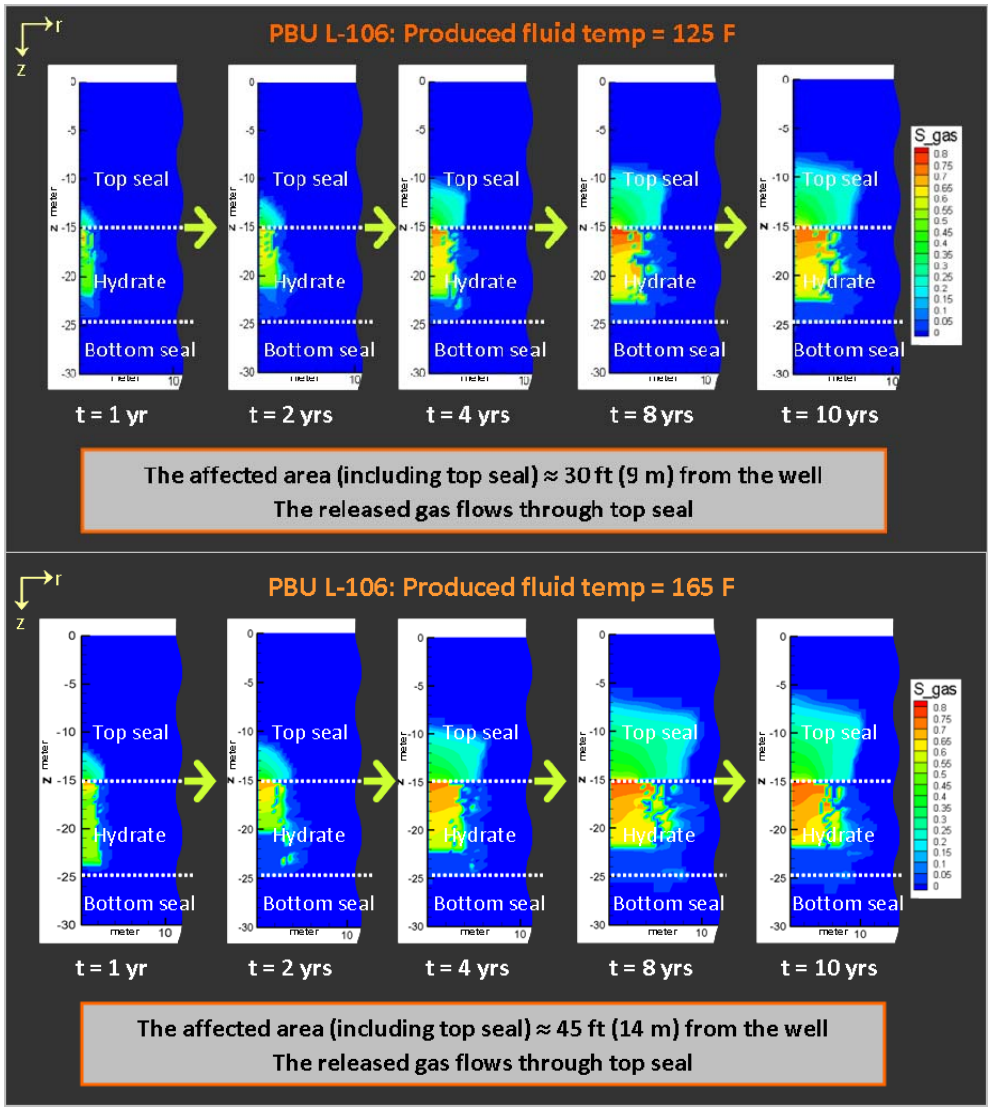

Figure 2-13: Gas saturation around well during production period

Pressures around the well in both cases do not significantly increase as the released gas can flow into the top seal (see Figure 2-14).

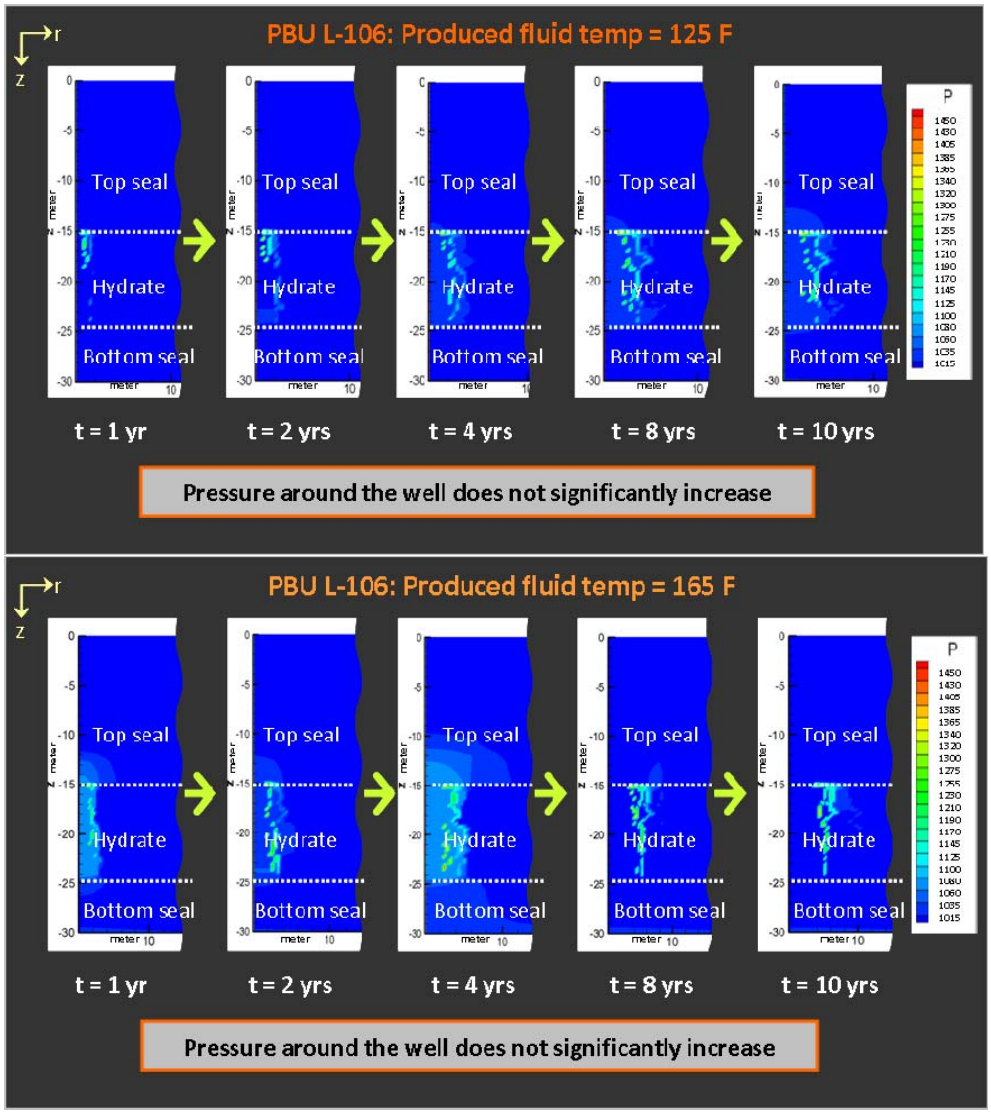

Figure 2-14: Pressure around well during production period

2.2.2 Case 2 ($k_{h\_Top\ seal}$ = 1 mD)

In this case, top seal horizontal and vertical permeabilities are 1 mD and 0.1 mD, respectively. As in the previous case, calculated in-situ permeability values in the hydrate-bearing layer are consistent with measured in-situ permeabilities measured in at Mt. Elbert #1.

Simulation Results

Figure 2-15 shows the temperature around the well during 10 years of production. The farthest affected distances in the two cases are not very different (115 ft and 125 ft), but near-well temperature (within 10 ft around the well) in the 165 ^{o}F case is slightly warmer than that in the 125 ^{o}F case.

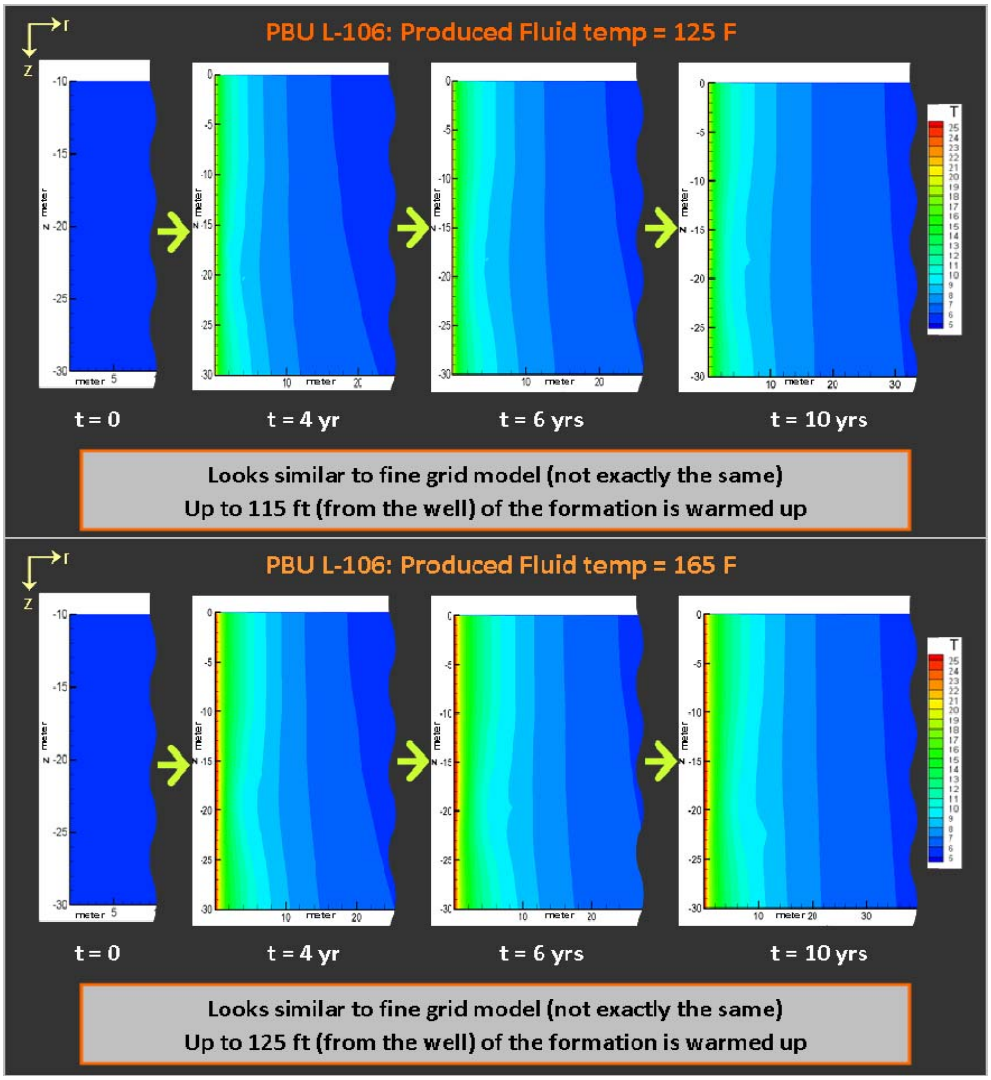

Figure 2-15: Temperature around well during production period

Hydrate saturations around the well for the 125 ^{o}F and 165 ^{o}F cases are significantly different (see Figure 2-16). The affected distances in the 125^{o}F and 165^{o}F cases are about 30 ft and 42 ft, respectively. The model predicts hydrate formation in the top seal when released gas moves into the top seal. Hydrate formation occurs higher in the top seal than in Case 1 (k_{h_top} seal = 0.1 mD), since released gas can move more easily into the higher permeability top seal.

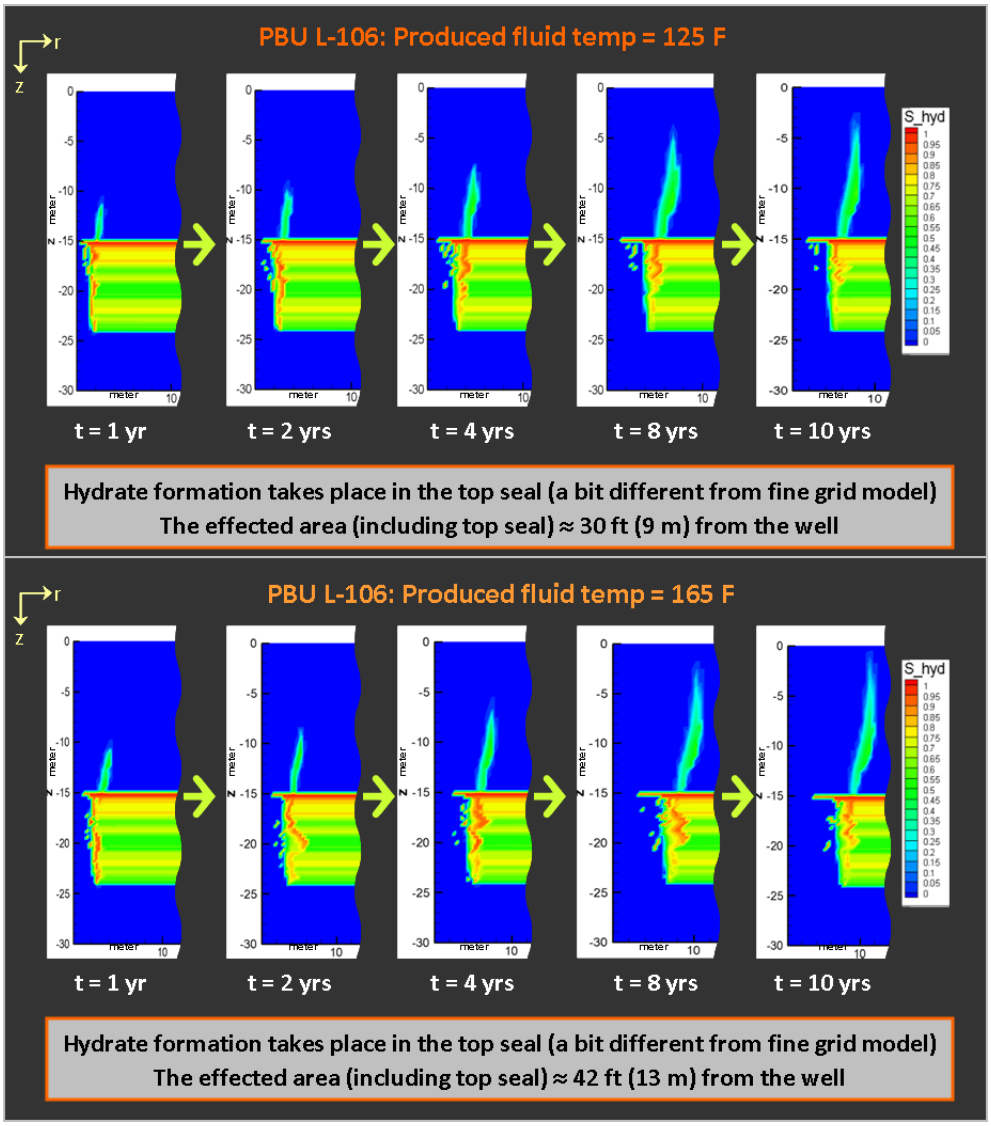

Figure 2-16: Hydrate saturation around well during production period

Gas saturations around the well for the two cases are significantly different (see Figure 2-17) as there is more hydrate dissociation in the 165 ^{o}F case. As a result, more gas is released in the hydrate-bearing layer and more gas migrates into the top seal and accumulates there. The released gas in this case can move higher into the top seal (50 ft) because the top seal permeability is higher than in Case 1 (23 ft).

As in Case 1, pressures around the well in both cases do not significantly increase, since gas released by hydrate dissociation can flow into the top seal (see Figure 2-17).

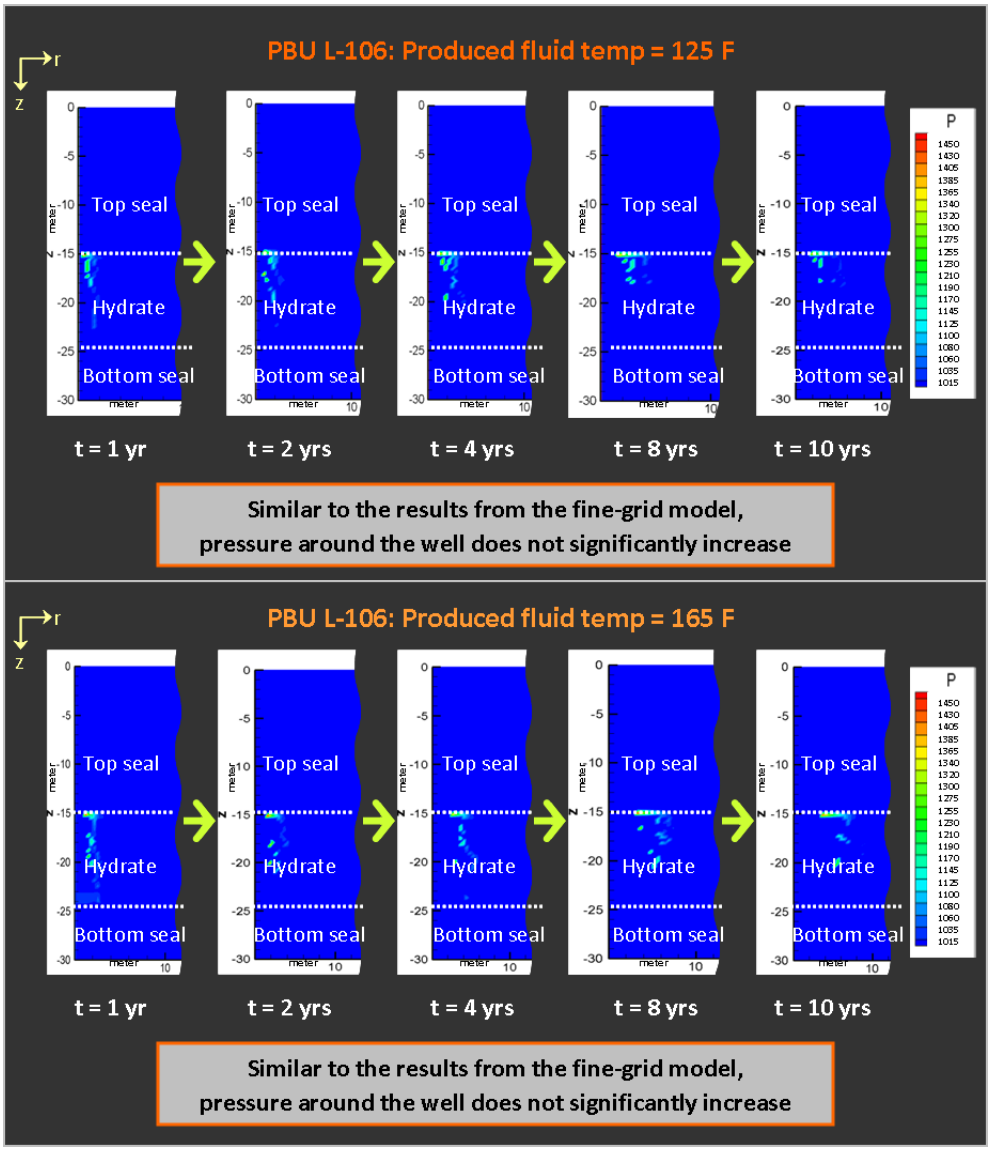

Figure 2-17: Pressure around well during production period

The affected distance (based on hydrate dissociation radius in the 165 ^{o}F case) in a vertical well system is approximately 45 ft from the well. The affected distance (based on hydrate dissociation radius) in a 45^{o} deviated well would be approximately 60 ft from the well (see Figure 2-18).

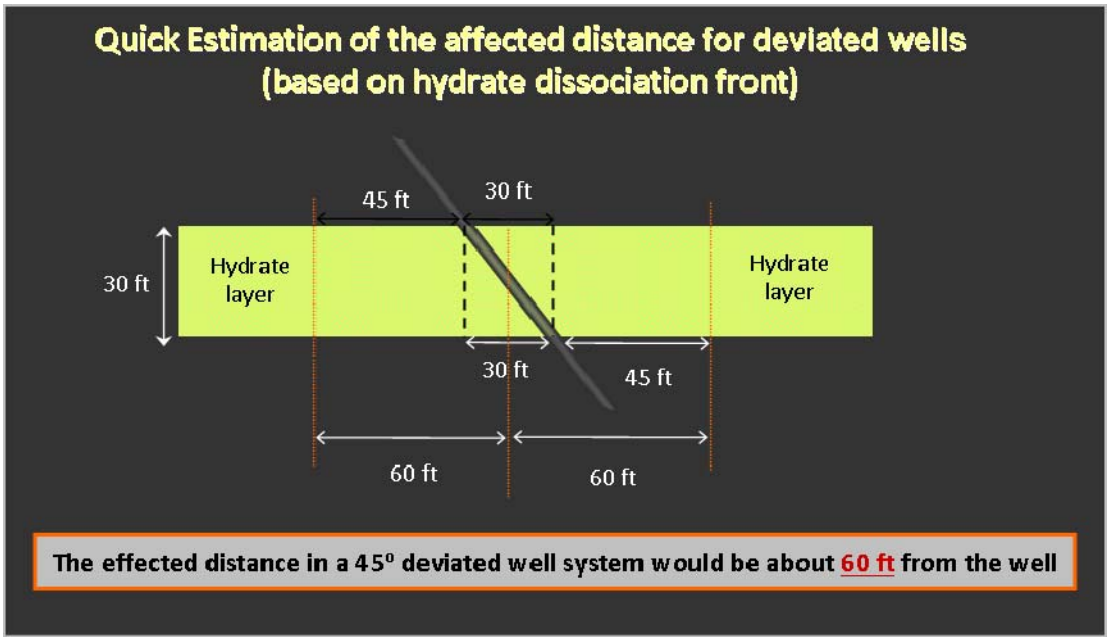

Figure 2-18: Quick estimation of affected distance in a 45° deviated well system

Conclusion

This simulation study shows that:

- The dissociation of near-wellbore hydrate takes place due to heat transfer from hot produced or injected fluid in the wellbore to the formation. Hotter fluid in the wellbore causes more and deeper heat transfer into hydrate-bearing strata.
- Based on hydrate dissociation radius in worst case scenario (165 °F and 0.1 mD top seal horizontal permeability), the affected distance is about 45 ft from the well in a vertical well system. The approximation of affected distance in a 45° deviated well (in a 30-ft thick hydrate interval layer) is about 60 ft from the well.

References Cited

Moridis, George J., and Michael Kowalsky, 2006, Depressurization-Induced Gas Production from Class 1 and Class 2 Hydrate deposits: Proceedings, TOUGH symposium 2006, Lawrence Berkeley National laboratory, pp 1-8

Mailloux, Jason, 2009, "Appendix C: Petrophysical Evaluation of Potential Hydrate-Bearing Wells on the North Slope of Alaska," *in* Schoderbek, David, Principal Investigator, Progress Report, Second Quarter 2009, ConocoPhillips Gas Hydrate Production Test (DOE Award No.: DE-NT0006553)

Appendix 3: Geocellular Model for Evaluation of Gas Hydrate Production Mechanisms in Selected Sandstones of the Sagavanirktok Formation near L-pad, Prudhoe Bay Field, North Slope of Alaska

Author: Mark Scheihing, ConocoPhillips Company, Anchorage, Alaska

Introduction

A geocellular model of gas hydrate-bearing sandstones of the Sagavanirktok Formation in a portion of the L-pad at Prudhoe Bay Field (Figure 3-1) was built to support reservoir simulation evaluation of dissociation and CO_2/CH_4 exchange production mechanisms for gas hydrate production. Simulation is underway in the Reservoir Mechanisms Group in ConocoPhillips Subsurface Technology in Houston, Texas.

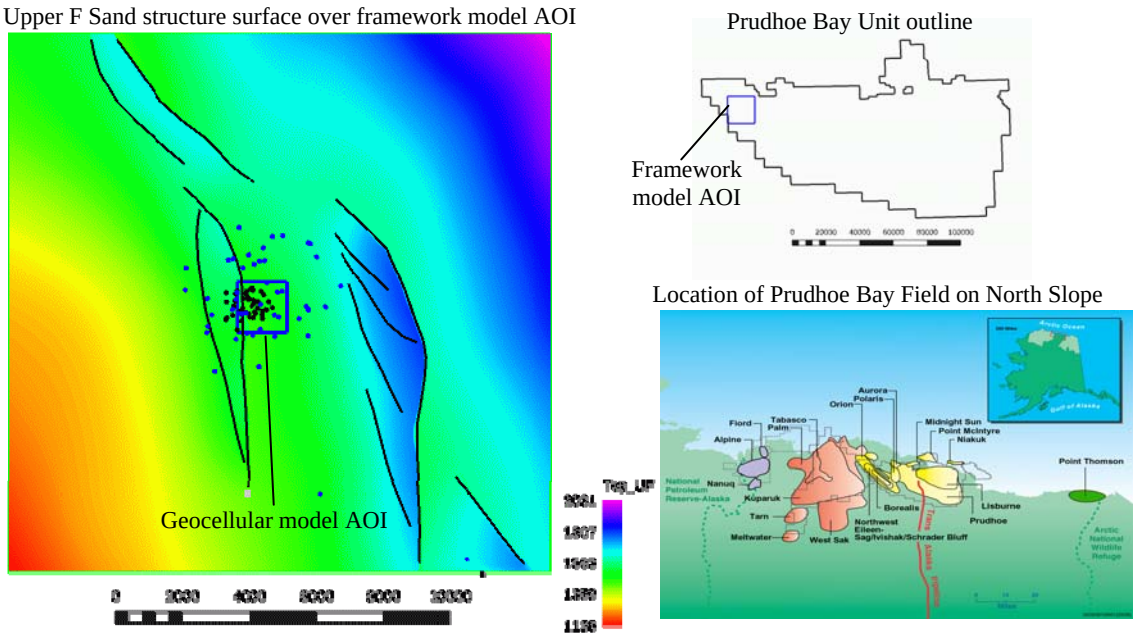

Figure 3-1 – Model AOI and well control shown on the Upper F Sandstone structure surface. Black points are well intersections at the top of the Upper F Sandstone, blue points at the top of the B Sandstone.

A structural and stratigraphic framework model was built across the Prudhoe Bay Unit L-pad area, delineating the informally named B through F sandstones. A 3D geocellular model was then constructed over the central part of this framework model, encompassing the B through D Sandstones. This model was rescaled to the 3D gridding requirements of the reservoir simulator and exported for use in gas hydrate process modeling. The model is constructed in Roxar's RMS version 2010.01.

Structural and Stratigraphic Modeling

A seismically defined structure grid of the top-most sandstone considered in this study, the Upper F Sandstone, was used as the basis for the 3D structural model. This grid, together with 10 fault surfaces, was interpreted and depth-converted. Structural surfaces

on deeper horizons were also interpreted and depth-converted but the top Upper F Sandstone is regarded as the most reliable for use in 3D structural modeling.

The original structure grid was conditioned to a subset of the well control in the L-pad area. The top of the Upper F Sandstone was picked in a total of 54 wells for which gamma ray logs are available. The original depth grid was conditioned to all wells with valid well picks and re-gridded with a smoothing filter and the fault surfaces to create a smoother structure grid with better defined fault scarps (Figure 3-2).

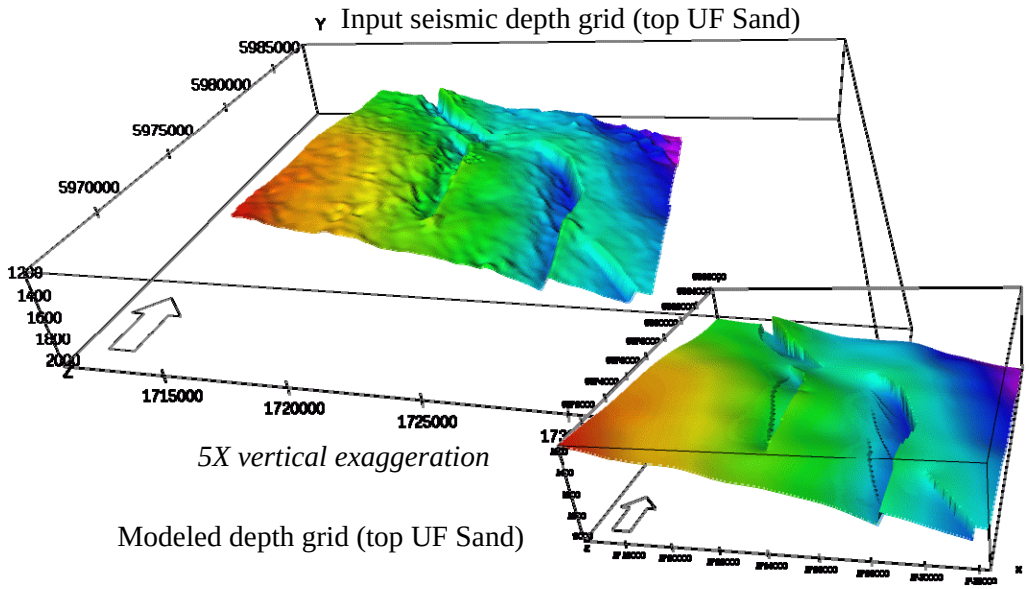

Figure 3-2 – Input vs. modeled top Upper F Sandstone structure grid.

A flow unit-scale reservoir zonation was established in this region, breaking out sand-rich and sand-poor intervals. Figures 3 and 4 show this stratigraphy on north-south and east-west-oriented sections, respectively, through the approximate center of the framework model AOI. Gross interval thicknesses are fairly consistent across the AOI. The reservoir stratigraphy attempts to constrain the sand- and siltstone-rich portions of upward-coarsening and fining sequences. A total of 12 zones are delineated, 6 of them sand-rich. Strata are labeled to conform with Sagavanirktok stratigraphic nomenclature proposed by of Collett (1993). Of these, the E, D and Upper and Lower C Sandstones are gas hydrate-bearing. The B and Upper and Lower F Sandstones are wet.

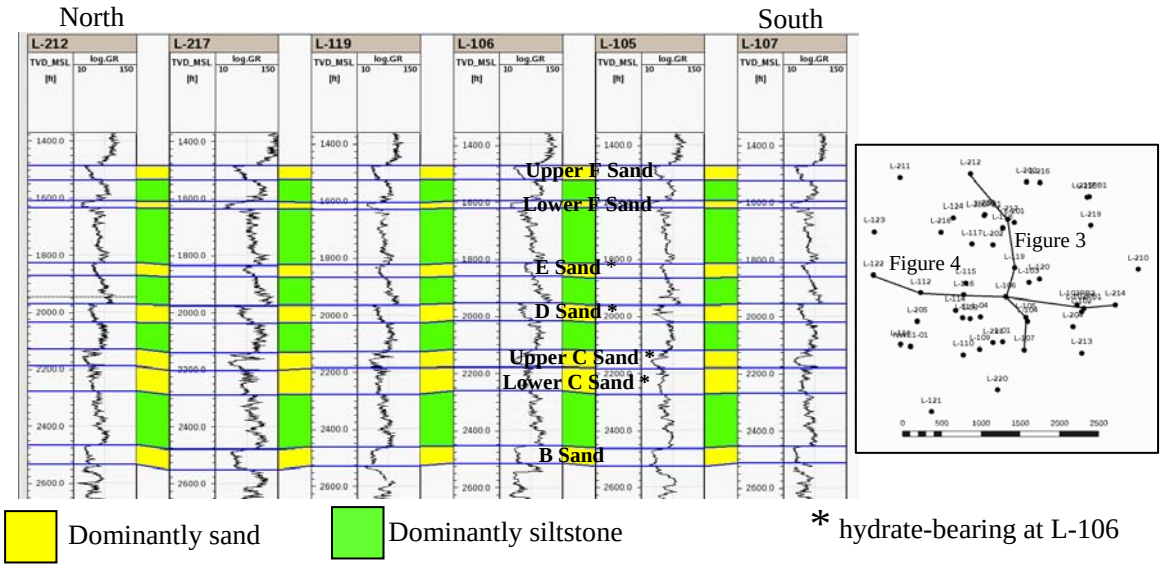

Figure 3-3 – North-south stratigraphic cross-section. Datum is top Upper F Sandstone.

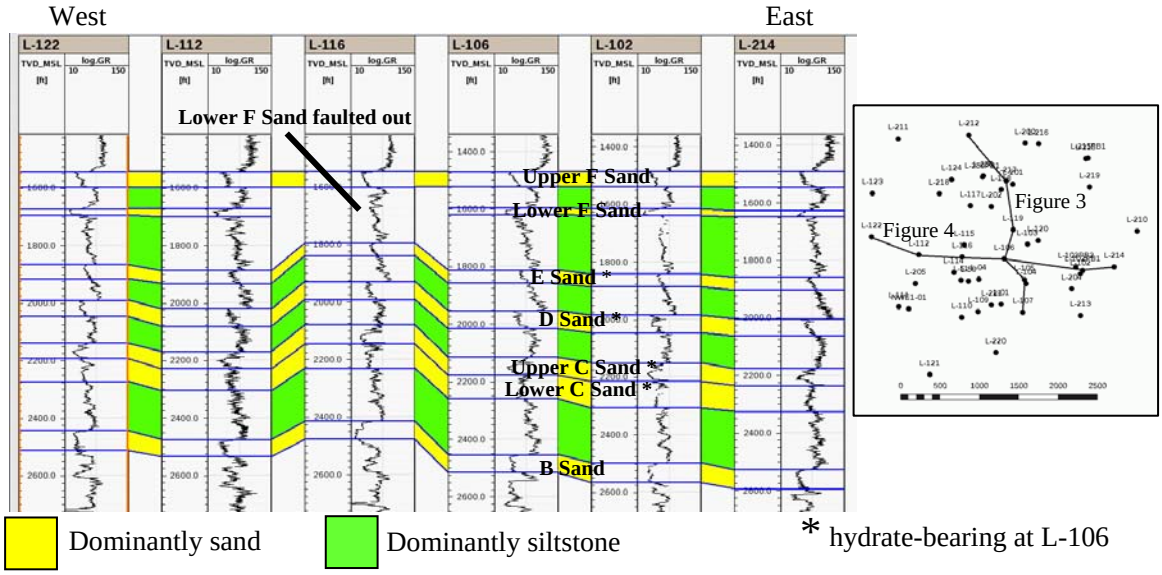

Figure 3-4 – East-west stratigraphic cross-section. Datum is top Upper F Sandstone.

The detailed zonation revealed the existence of faulted sections within a number of the wells (see Figure 3-4 for an example). Point sets of fault cuts in wells (called "HardPoints") were generated and used together with the seismically interpreted fault surfaces (converted to fault sticks) in fault modeling. Some "pseudo-fault picks" were also added to the HardPoints set to help keep wells on the correct side of the faults.

Isochore thickness well picks were used to generate gross thickness isochore grids. Only wells with complete intervals (that is, not faulted) were used to generate the gross thickness isochore grids to avoid thickness anomalies associated with faults. The isochore grids were used, together with depth well picks, the Upper F Sandstone structure surface and modeled fault surfaces, to create the other stratigraphic horizons using the

Horizon Modeling functionality in RMS 2010.01. Table 1 is a summary of the input date used in horizon modeling to generate the framework model. In effect, horizon modeling involves adding down gross thickness isochore grids from the top upper F seismically defined structure surface while honoring the zone tops and fault model.

Element Modeled	Input Data			
	Well picks	Filtered structure surface	Fault model	Isochores
Horizons	Hard	Soft	Soft	0.9 confidence

Table 3-1 – Input data used in horizon modeling. "Hard" indicates that data are exactly honored; "soft" indicates that data are not necessarily exactly honored. Value of 0.9 indicates high degree of conformance with the input gross thickness isochore grids.

A representative east-west structural cross-section is shown in Figure 3-5. The framework model is about 16,000 x 16,000 feet areally and about 1,045 feet thick from the top of the Upper F Sandstone to the base of the B Sandstone. Minimum depth in the model is 1136 feet and maximum depth is 3025 feet SSTVD.

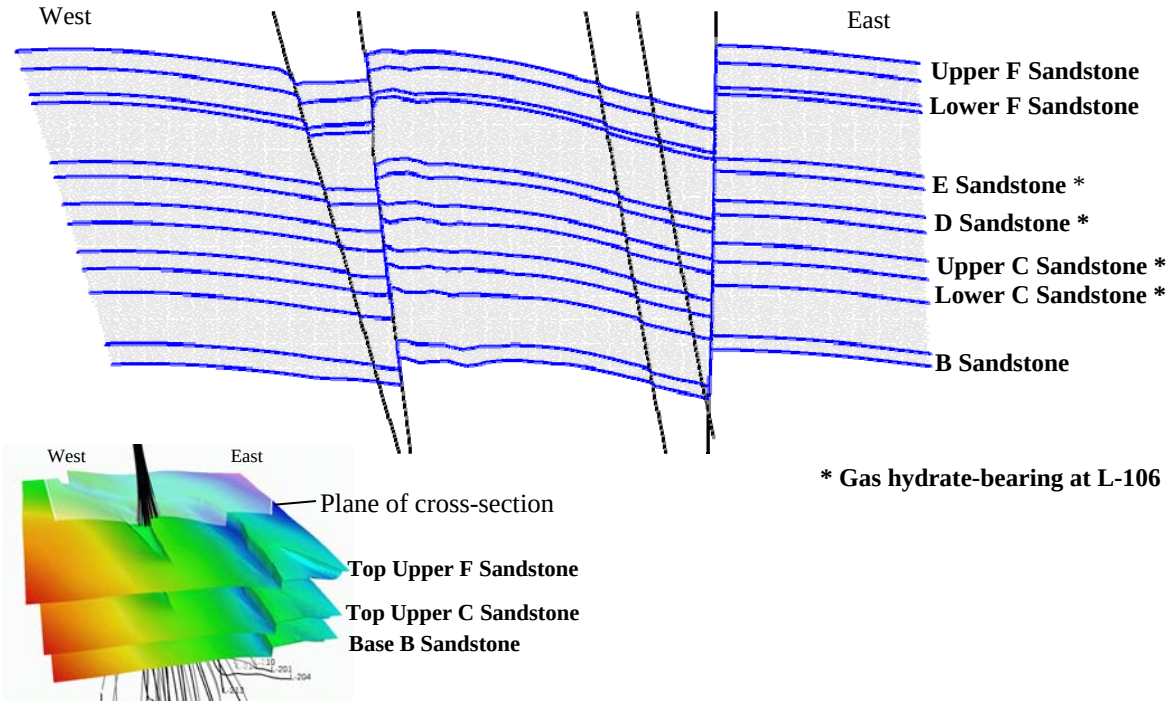

Figure 3-5 – East-west-oriented structural cross-section across the framework model.

This framework model provides the subdivided "tank" that serves as the basis for a 3D grid anywhere within the framework model volume.

3D Geomodel and Simulation Gridding

The AOI of the 3D simulation grid is centered on BP's proposed gas hydrate well location, but also encompasses the COP proposed location. The model AOI is 1500 x 1500 feet (Figure 3-6). Stratigraphically, the model includes the gas hydrate bearing D

Sandstone and Upper and Lower C Sandstones and extends down to the base of the wet B Sandstone, a vertical distance of about 550 feet. The western margin of the model is constrained by the major north-south bounding fault cutting across the L-pad.

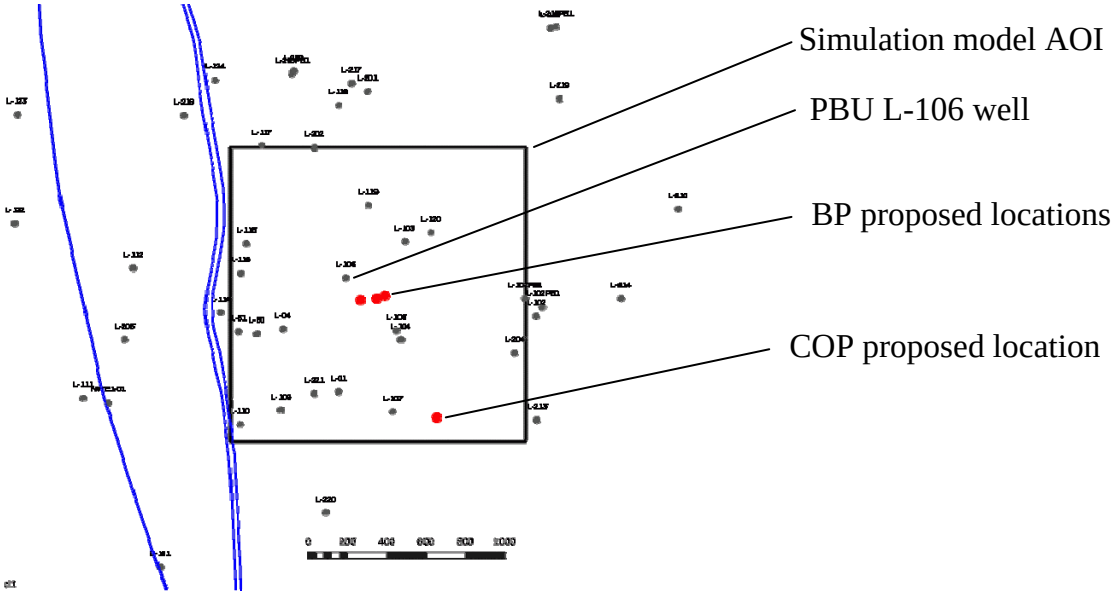

Figure 3-6 – Geocellular model AOI together with well intersections at top Upper C Sandstone and proposed BP and COP gas hydrate production well locations.

The specific processes to be modeled for this project require both an areally and vertically non-uniform grid, in which the center of the model is gridded to a much higher resolution than the model periphery. Vertically, the principal gas hydrate-bearing sandstone of interest, the Upper C Sandstone, requires the finest layering. The 3D simulation grid was constructed first. Then the 3D "fine-grid" geocellular model was designed in order to be readily rescaled into the simulation grid.

The areal grid layout of the simulation grid is shown in Figure 3-7. The areal grid block size varies from about 6x6 foot grid blocks in the center of the model to 50x50 foot grid blocks in the periphery of the model.

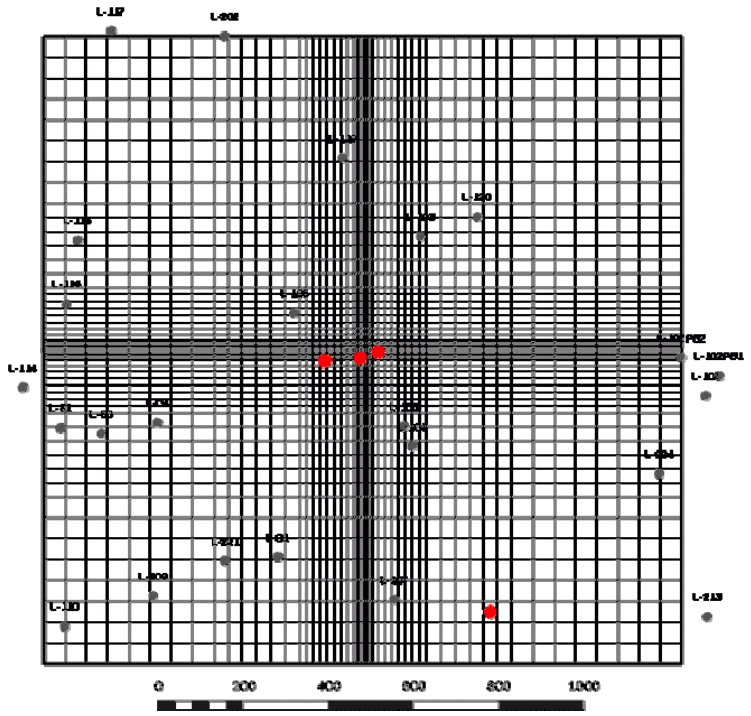

Figure 3-7 – Simulation areal grid layout.

Layer thicknesses vary from about 3 feet thick in the Upper C Sandstone which is the primary production target in L-pad to 23 feet in the Lower C siltstone zone (Figure 3-8). There are a total of 81 layers and 210,681 cells in the resulting 3D simulation model.

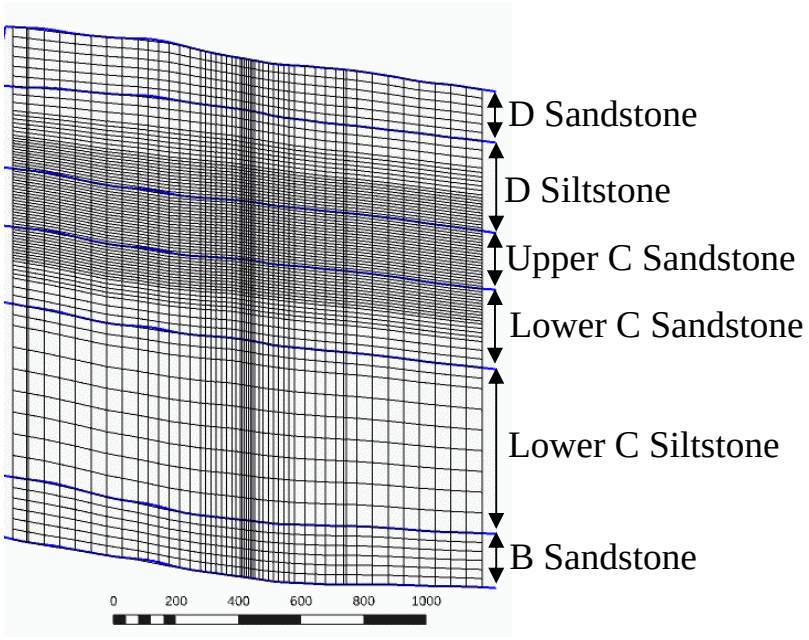

Figure 3-8 – Layering in simulation model.

In designing fine-grid geocellular and simulation model grids, it is generally regarded as good practice *not* to areally upscale the fine-grid geocellular model. Thus, the areal grid layout of the geocellular and simulation model is generally kept the same. This works well in cases in which the areal grid block size is uniform across the model AOI. However, for this model, a decidedly non-uniform areal grid layout is required. It is not possible to distribute properties within a grossly non-uniform grid as it produces unacceptable properties distributions. As an example, Figure 3-9 shows the effect of distributing porosity within the areally non-uniform grid.

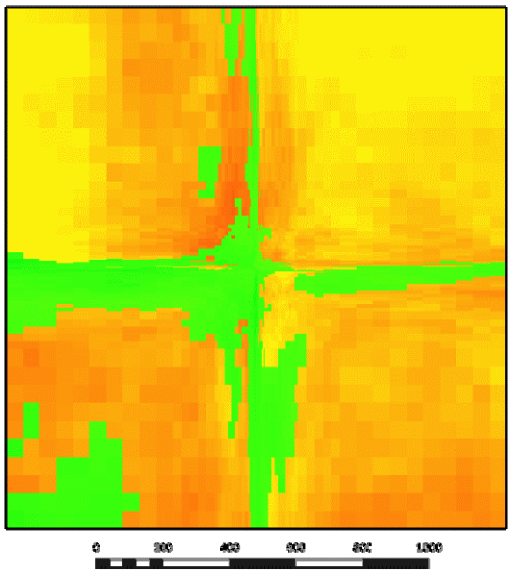

Figure 3-9 – Porosity distributed within a non-uniform grid. Note the property distribution artifact created by the non-uniform areal grid..

In order to create an areally reasonable distribution of properties, a uniform grid block size of 100 x 100 feet was created for the "fine-grid" geocellular model. After properties distribution, this 100 x 100 foot areal grid block size was globally refined to the non-uniform simulation grid layout. Layering remained the same. This preserves the spatial distribution of properties within the uniform grid but refines the model areally as required for reservoir simulation. Figure 10 shows the porosity distribution within uniform 100 x 100 foot grid block beside the globally refined non-uniform grid block layout for layer 5 in the model.

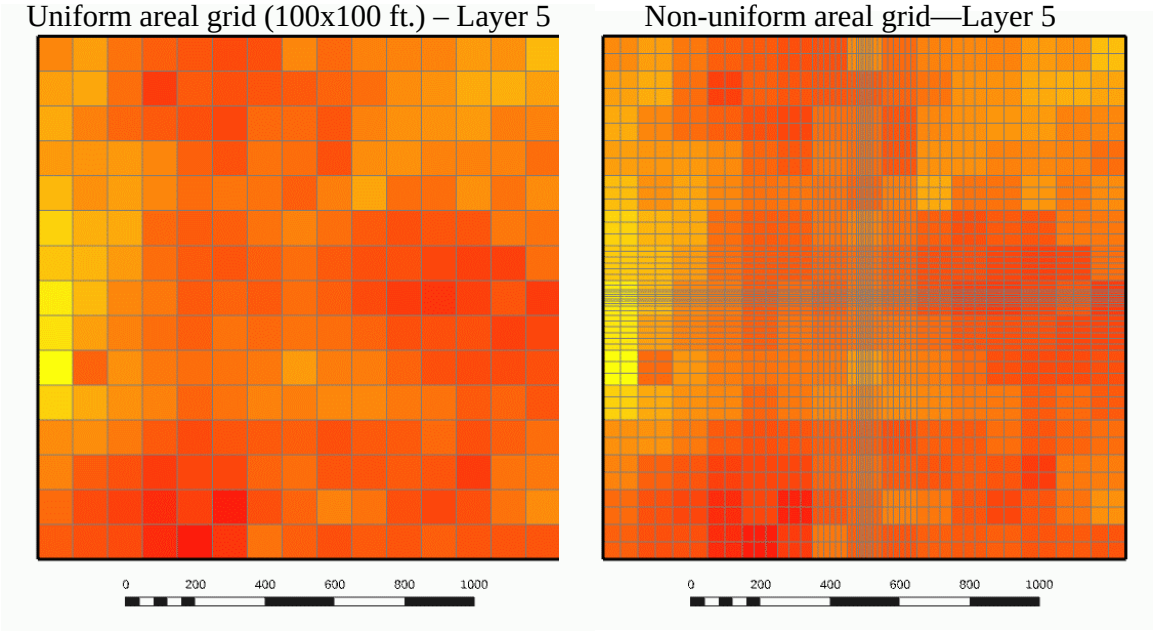

Figure 3-10 – Porosity distribution for layer 5 in the uniform and non-uniform fine-grid model.

In the fine-grid geocellular model, all zones are layered at a resolution of about 1 foot using proportional gridding. The exact number of layers in each zone was adjusted so that it was a simple multiple of the total number of layers in each zone in the simulation grid. Table 3-2 shows a comparison between the layering in the fine grid model and simulation model. The fine-grid model was then uplayered into the simulation model using conventional uplayering techniques (see section on "Model uplayering and export of parameters" below). The uniformly gridded, fine-grid geomodel contains 548 layers and 123,300 cells. The non-uniformly gridded, fine-grid geomodel contains the same number of layers and 1,425,348 cells.

Zone	Geomodel	Simulation model
D Sandstone	60	6@10ft.
D Siltstone.	84	3@9ft.
		6@5ft.
		12@3ft.
UC Sandstone	60	20@3ft.
LC Sandstone	95	12@3ft.
		4@5ft.
		3@9ft.
LC Siltstone	189	2@12ft.
		7@23ft.
B Sandstone	60	6@10ft.

Table 3-2 – Layering of the fine-grid geocellular and simulation models. N@Zft. refers to the number of layers at a certain average layer thickness in the simulation grid..

Properties Distribution

The reservoir simulation model requires the following properties:

1) Total porosity at simulated overburden stress
2) Absolute air permeability (horizontal and vertical) at simulated overburden stress and Klinkenberg-corrected)
3) Gas hydrate saturation
4) Water saturation
5) Irreducible water saturation as a per-zone average

For this model, total porosity comes from computed porosity logs using ConocoPhillips' in-house log model, modified for shallow, unconsolidated sandstones. Neutron density log availability is limited for L-pad wells, so porosity is based on the gamma ray log, calibrated to neutron-density porosity for wells with both logs. Absolute air permeability is derived from a porosity transform based upon Mt. Elbert core data. Gas hydrate saturation is calculated using Archie's and AIM techniques based upon the L-106 well. Irreducible water saturation is based upon a relationship between CMR log bins and volume clay in the Mt. Elbert well. More detail on each of these data types and sources is given in the relevant sections below. In addition, although not directly an input into the reservoir simulation model, rock type was also calculated, since porosity and permeability are both functions of rock type.

Rock type modeling: The interval encompassing the Upper F Sandstone to B Sandstone is characterized as a bimodal system of very fine-grained unconsolidated sandstones and unconsolidated siltstones. For a given depth of burial, these two rock types control the distribution of porosity and permeability. Of course, in such unconsolidated sediments, porosity and permeability also vary with depth because of compaction, but within a given depth range, rock type is the primary control.

The flow unit-scale zonation provides a first order grouping of porosity and permeability, but both sandstones (RXTP=1) and siltstones (RXTP=0) can occur within the same zone. Therefore, it is necessary to first distribute rock types before distributing petrophysical properties within them.

A rock type log was created using the porosity log. Histograms of porosity from the porosity log model are strongly bimodal (Figure 3-11) and correspond to rock type.

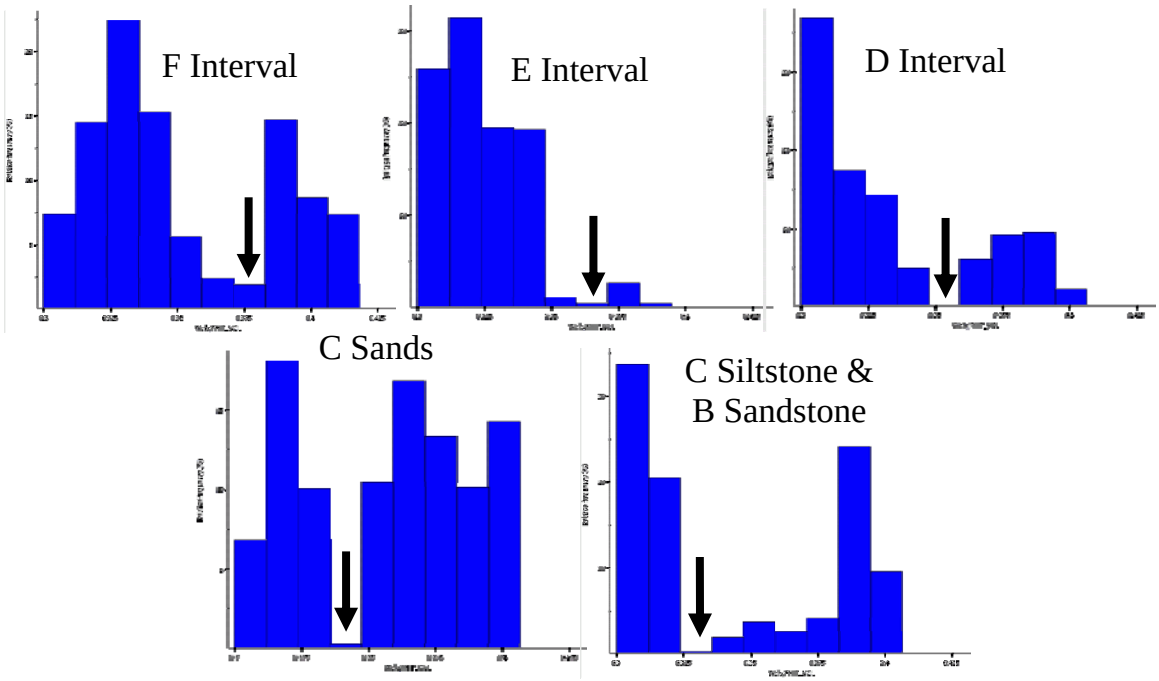

Figure 3-11 – Histograms of the porosity log by individual or group zones. Note that the break (arrows) between the sandstone and siltstone distributions systematically shifts to lower porosities from the F interval (shallowest) to the B Sandtone (deepest) as a function of increased compaction over about 1000 feet of depth.

Given this bimodal relationship and strong correlation to rock type, zone-based porosity cutoffs were used to distinguish sandstone (RXTP=1) from siltstone (RXTP=0). The value of the cutoff decreases with depth as a function of overall reduction of porosity from increasing compaction. Table 3 shows the cutoffs used for each zone in the model.

Zones	Porosity Cutoff
Upper F Sandstone	0.38
Upper F Siltstone & Lower F Sandstone	0.375
Lower F Siltstone	0.370
E Sandstone & E Siltstone	0.360
D Sandstone	0.357
D Siltstone	0.355
Upper C Sandstone	0.348
Lower C Sandstone	0.346
Lower C Siltstone	0.335
B Sandstone	0.330

Table 3-3 – Porosity cutoffs used to define rock types. Porosity > cutoff = RXTP1 and porosity < cutoff = RXTP0

An example of the resulting rock type log is shown in Figure 3-12.

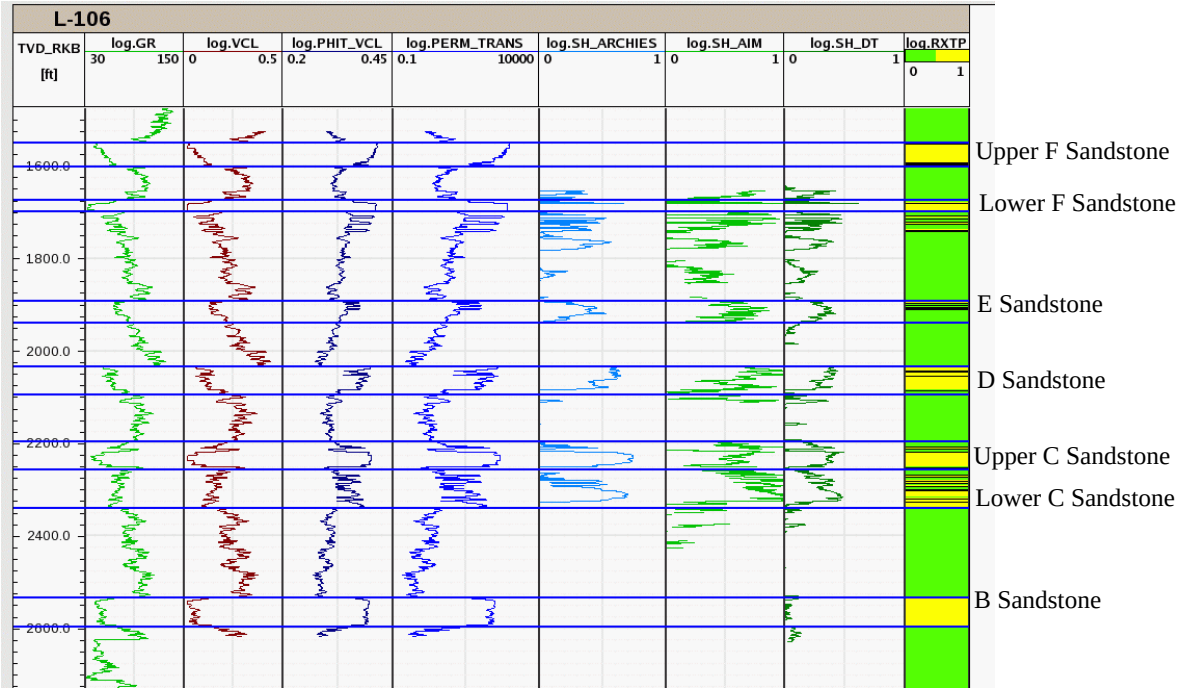

Figure 3-12 – Example of rock type log in L-106 shown with other open hole and calculated logs from the ConocoPhillips in-house "Shallow, Unconsolidated" log model.

Within the AOI of the model, the most significant trend is the vertical variation in proportion of rock types. Areal variation is more limited. In order to capture this vertical variation, a vertical proportion curve (VPC) was calculated from high-graded blocked wells and used in Sequential Indicator Simulation (SIS) to distribute rock types. Figure 3-13 shows the VPC that was used as 1D trend information in the SIS. Wells that had suspect gamma ray logs, leading to vertical distributions of rock types 1 and 0 that are clearly off-trend from offset well control were not used in either the VPC or subsequent properties modeling.

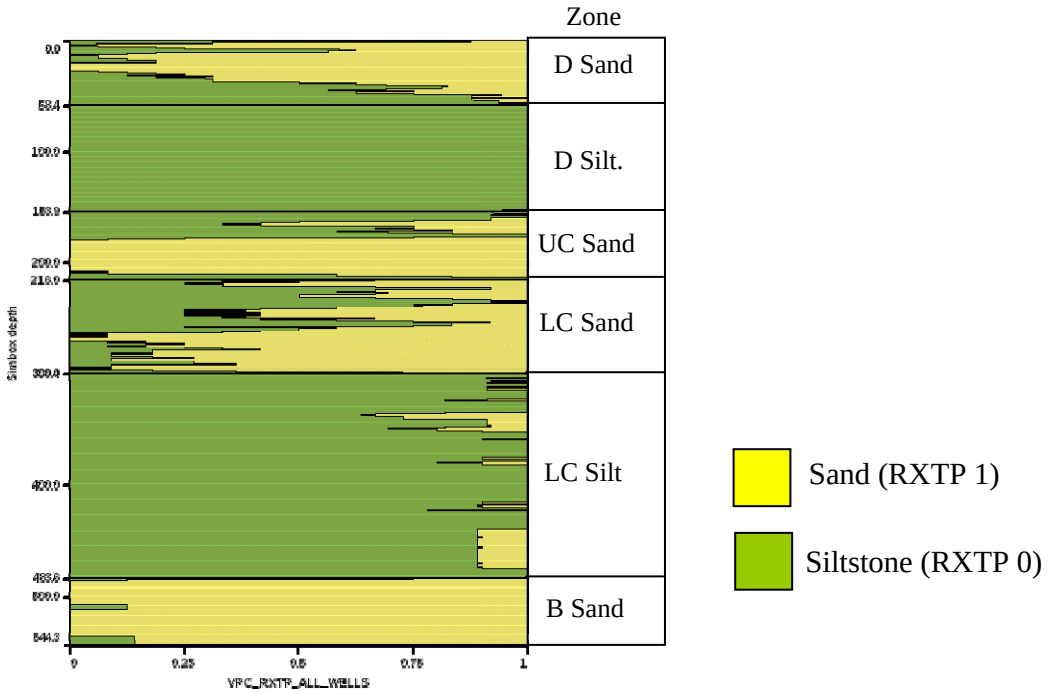

Figure 3-13 – Vertical proportion curve of Rock types 0 and 1 based upon the blocked wells.

A horizontal variogram range of 3000 feet was used for both the main and perpendicular directions. A vertical variogram range of 1.0 foot was used. Figure 3-14 shows the resulting rock type realization through the center of the model. Comparison of the VPC and rock type realization shows that the SIS modeling reproduces the input vertical rock type proportions trends very well, capturing the main vertical sandstone and siltstone distribution trends.

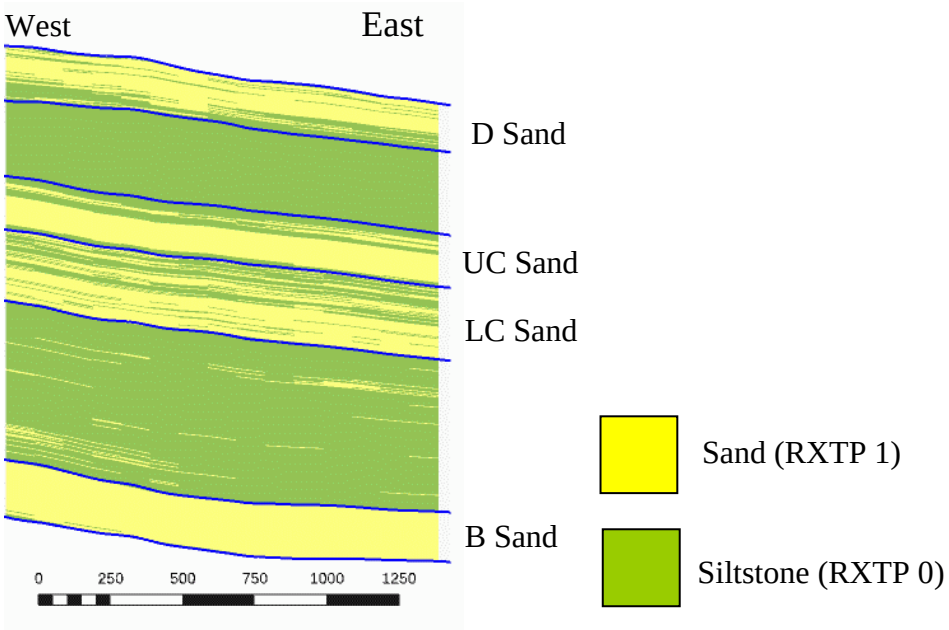

Figure 3-14 – East-west cross section through rock type realization. 3X vertical exaggeration.

A 3D trend parameter was also generated using the VPC and grid of areal rock type proportions for each zone and used in another SIS run. However, the result was less satisfactory in reproducing the most important vertical rock type trends and, thus, was not further pursued.

The rock type realization based upon the VPC as 1D trend data then served as the basis for distributing petrophysical rock properties as described below.

Porosity modeling: Porosity was modeled using Sequential Gaussian Simulation (SGS) on a by-zone and by-rock type basis. The rock type realization described in the previous section was used as a template for distributing porosity. The same variogram ranges as used in rock type modeling were used in porosity modeling. In order to reinforce vertical trends in porosity, a vertical depositional trend was used in the porosity transformation sequence. For each zone and rock type, the transformations applied to the porosity distribution are as follows:

Truncation:	Keep data and realizations above 0
Mean:	Shift to mean of data
Depositional trend:	Apply vertical porosity trend
Skewness reduction:	Apply normal score transformation

The resulting porosity distribution is shown in Figure 3-15. The contrast in porosity between sandstones and siltstones is evident and the vertical trend in porosity is preserved in the realization.

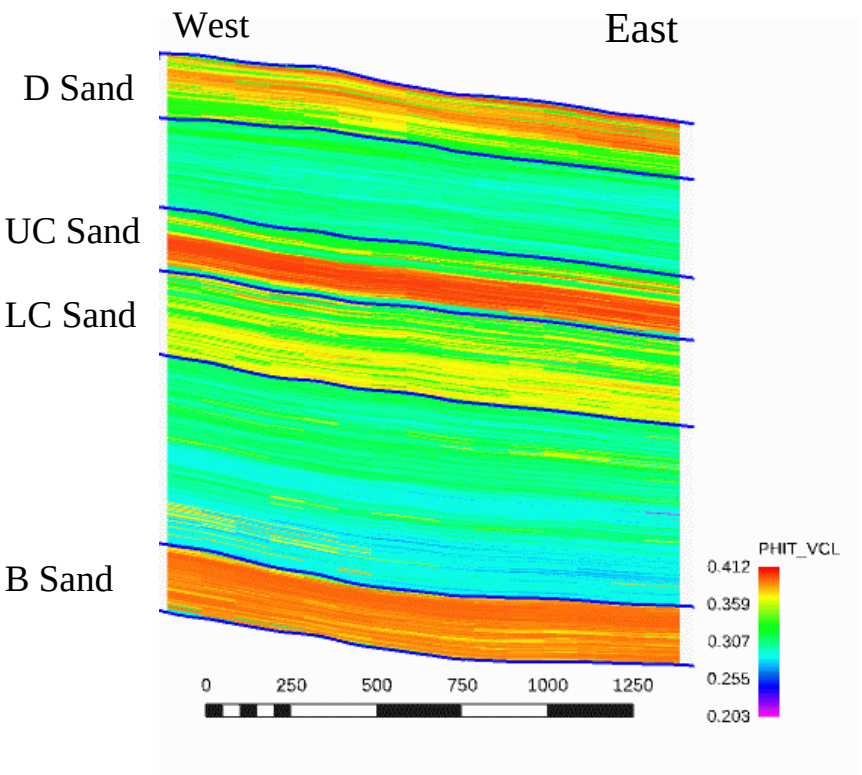

Figure 3-15 – East-west cross section through porosity realization. 3X vertical exaggeration.

Permeability modeling: Lacking core in the L-pad within the Sagavanirktok Formation, it was decided to use high-graded Mt. Elbert core plug data as the basis for establishing a transform between porosity and permeability. High-graded overburden and Klinkenberg-corrected core plug data were used to develop a regression between porosity and permeability (Figure 3-16).

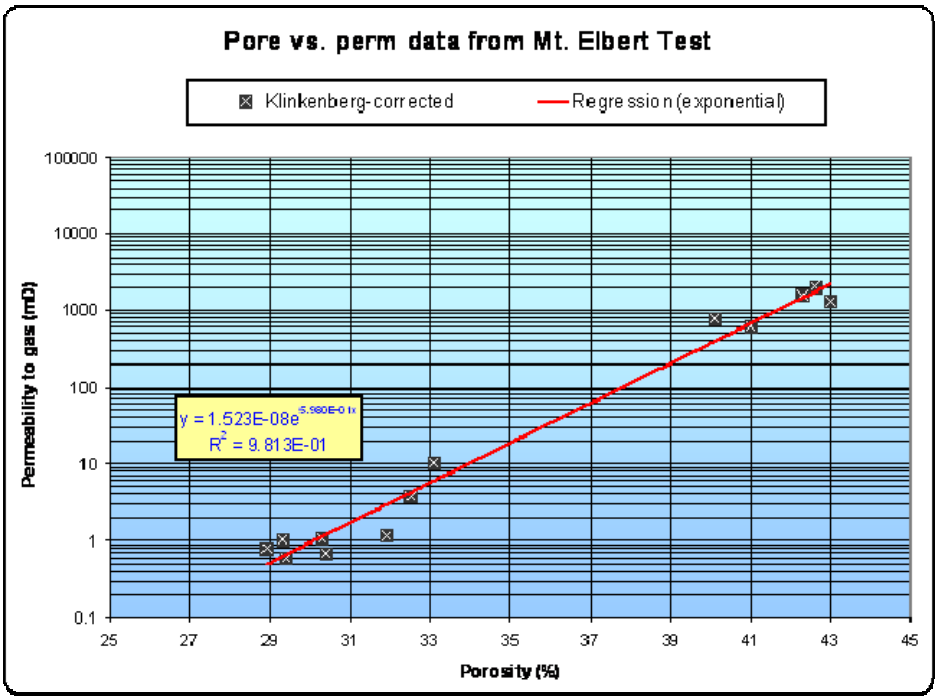

Figure 3-16 – Mt. Elbert #1 core plug poro-perm cross-plot.

The core plug data were high-graded to remove clearly anomalous measurements before the regression was calculated. There are an insufficient number of samples to support the calculation of a Swanson's mean for the dataset, but the fit to the data is tight enough such that this should not be necessary.

Horizontal permeability in the model was then simply calculated from porosity using the regression. To maintain the relationship between porosity and permeability in the simulation model, permeability was calculated from porosity in the uplayered simulation grid as well as the geocellular model grid. Vertical permeability was estimated by multiplying the horizontal permeability by 0.1. The value of 0.1 was chosen to be consistent with that used in previous simulation work.

Gas hydrate and water saturation modeling: In PBU L-106, the D Sandstone and Upper and Lower C Sandstones are hydrate-bearing. The B Sandstone is wet. Gas hydrate saturation logs, calculated by several different techniques, are available for the L-106 well based on work summarized in Mailloux (2009). There are basically four techniques that are used to calculate S_h: Archie's, AIM (Advanced Interpretation Module - a simultaneous equation solver), sonic (DT) and NMR. Since no NMR logs are available

for L-pad wells, only the first three were calculated for the L-106 well (see Figure 3-13), the only well with the requisite open hole logs for these calculations.

The DT method grossly underestimates S_h in the L-106 well, so was not used in modeling. The AIM method tends to give much higher S_h, particularly in the Lower C Sandstone. Both the Archie's and AIM estimates of S_h were modeled and provided for use in the simulation model.

S_h for both the Archie's and AIM methods was distributed using SGS on a by-zone and by-rock type basis. As in the case for porosity, a vertical depositional trend was used in the transformation sequence to better represent vertical variations in Sh. Also, as in the case for porosity, the rock type realization was used as the template for distributing S_h using both the Archie's and AIM S_h calculations. Figure 3-17 shows both the Archie's and AIM realizations together.

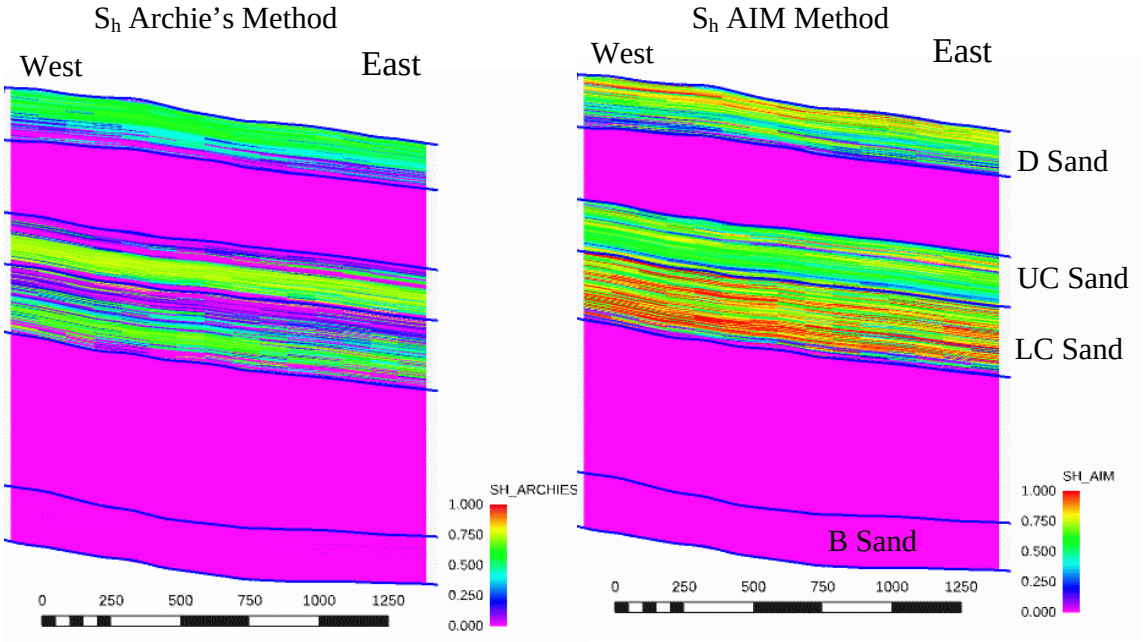

Figure 3-17 – East-west cross sections through Archie's and AIM gas hydrate saturation realizations. 3X vertical exaggeration.

Irreducible water saturation calculation: The reservoir simulator requires an average irreducible water saturation for each zone rather than a 3D parameter in the model. However, no capillary pressure data exist for either L-pad wells nor for the Mt. Elbert cored interval with which to estimate S_{wir}. However, the Mt. Elbert well has a CMR log with binned porosity data based upon relaxation time ranges. Bins 1 through 3 correspond to the shortest relaxation times associated with clay- or capillary-bound water. The first three bins were summed and converted to S_{wir} by dividing by total porosity. These were then cross-plotted against wireline log-based volume clay (Figure 3-18) and the following relationship developed between the two:

$$SWIR = b1 + \exp^{b2 + (b3/VCLY)}$$

Where: b1 = 0.055555
b2 = 0.71111
b3 = -0.58888

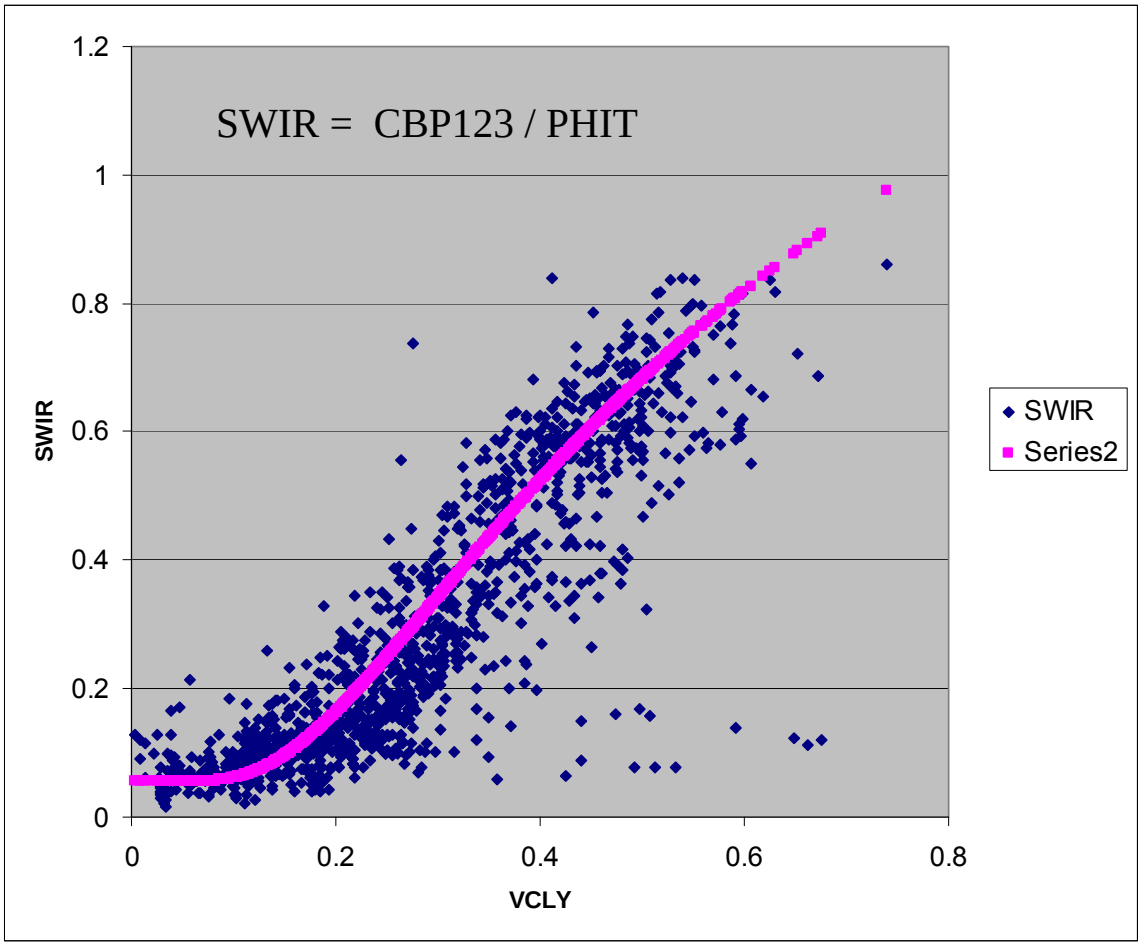

Figure 3-18 – Swir / VCLY cross-plot.

This relationship then provided a means for estimating S_{wir} from VCLY in L-pad wells. This relationship was applied to the blocked wells within the model AOI and average S_{wir} for both the sandstone and siltstone and sandstone alone computed for each zone in the model (Table 4).

Zone Number	Zone	Avg. Swir for zone	Avg. Swir for sandstone only
1	D Sandstone	0.10	0.07
2	D Siltstone	0.32	---
3	Upper C Sandstone	0.12	0.07
4	Lower C Sandstone	0.11	0.08
5	Lower C Siltstone	0.25	---
6	B Sandstone	0.06	0.06

Table 3-4 – Average S_{wir} by zone for both the entire zone (sandstone and siltstone) and sandstone component only.

The resulting S_{wir} values are reasonable for such unconsolidated sediments. For the siltstone/mudstone-rich zones, S_{wir} values are low, but these intervals generally contain higher proportions of silt than clay.

Model uplayering and export of parameters

As previously stated, the areally non-uniform geomodel was uplayered into a simulation grid with an identical non-uniform areal grid layout. In the sandstones, porosity was uplayered using arithmetic averaging with a net volume weight. Gas hydrate saturation was uplayered using arithmetic averaging with a net pore volume weight. In the siltstone zones, no weighting was applied, as sand percentage is extremely low. Water saturation was obtained by 1-Sh. Horizontal permeability was calculated from the uplayered porosity using the transform previously discussed. Vertical permeability was calculated from the horizontal permeability by multiplying the horizontal permeability by 0.10, as previously discussed. Figure 3-19 shows a comparison between porosity in the finely layered geomodel and the uplayered reservoir simulation model.

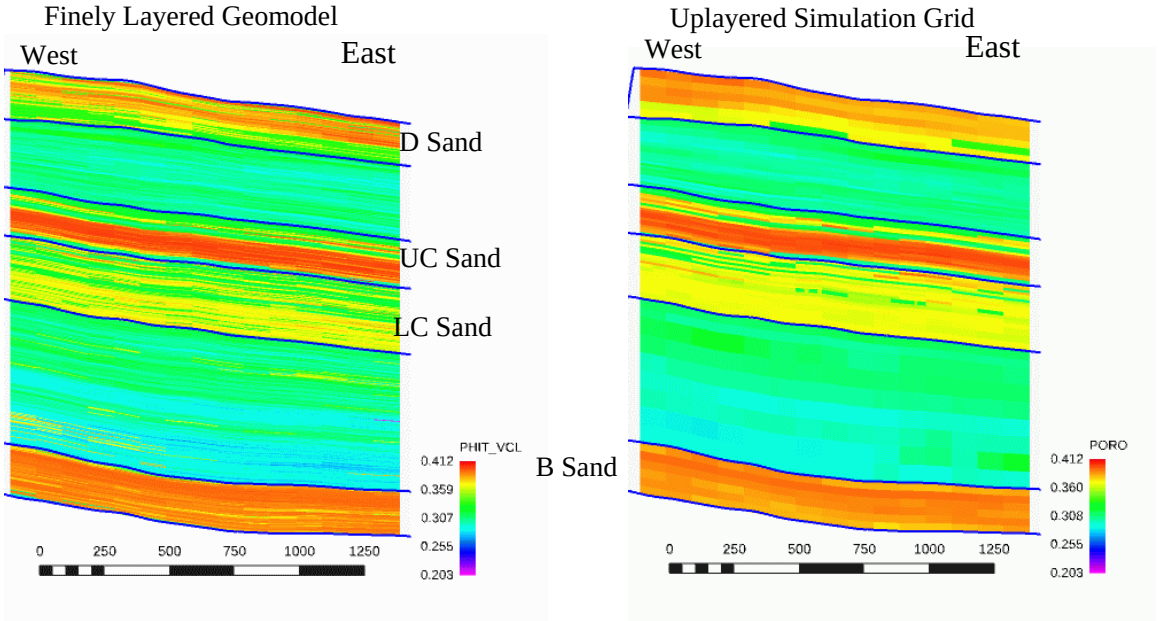

Figure 3-19 – Comparison between east-west cross section through finely layered geomodel and uplayered simulation grid. 3X vertical exaggeration.

The reservoir simulator being used for evaluating gas hydrate production mechanisms does not use conventional corner point grid descriptions such as the Eclipse grid GRDECL format. Instead, the grid description provided consists of dX, dY, dZ, topZ and zone number (1 through 6), exported as individual files. The complete set of outputs is summarized in Table 3-5.

Parameter	Category	Description
X_increment	Grid description	X coordinate increment in NAD83
Y_increment	Grid description	Y coordinate increment in NAD83
Z_increment	Grid description	Z coordinate increment in NAD83

Z_top	Grid description	Topmost Z value of model in NAD83
SUBGRID	Grid description	Zone (1 through 6)
PORO	Property parameter	Uplayered total porosity
PERMX_transform	Property parameter	Horizontal permeability from transform
PERMV_transform	Property parameter	Horizontal permeability * 0.1
NETSAND	Property parameter	Net sand percentage in cell
SH_AIM	Property parameter	Uplayered gas hydrate saturation using AIM
SH_ARCHIES	Property parameter	Uplayered gas hydrate saturation using Archie's
SW_AIM	Property parameter	1 - uplayered AIM gas hydrate saturation
SW_ARCHIES	Property parameter	1 - uplayered Archie's gas hydrate saturation

Table 3-5 – Exported grid description and property parameters for use in reservoir simulator.

Model property statistics are summarized in Tables 6 and 7 below.

Zone	Porosity				Horizontal Permeability				Vertical Permeability			
	Avg.	Std.	Min.	Max.	Avg.	Std.	Min.	Max.	Avg.	Std.	Min.	Max.
1*	0.38	0.018	0.28	0.41	136	63	3.00	307	13.6	6.3	0.30	30.7
2†	0.31	0.006	0.29	0.33	1.38	0.50	0.41	4.28	0.138	0.050	0.041	0.428
3*	0.39	0.036	0.29	0.41	265	151	0.65	557	26.5	15.1	0.065	55.7
4*	0.37	0.019	0.30	0.40	59	37	0.78	443	5.9	3.7	0.078	44.3
5†	0.30	0.010	0.28	0.37	1.46	1.33	0.30	60	0.146	0.133	0.030	6.0
6*	0.39	0.004	0.36	0.40	197	47	43	289	19.7	4.7	4.3	28. 9

Table 3-6 – Simulation grid statistics by zone for porosity, horizontal and vertical permeability. * indicates net volume weighted averages used for zone; † indicates bulk volume weighted averaged used for zone.

Zone	Sh Archie's				Sh AIM				Net Sand			
	Avg.	Std.	Min.	Max.	Avg.	Std.	Min.	Max.	Avg.	Std.	Min.	Max.
1	0.52	0.17	0	0.84	0.66	0.36	0	1	0.60	0.34	0	1
2	0	0	0	0	0	0	0	0	0	0	0	1
3	0.64	0.29	0	0.84	0.6	0.17	0	1	0.61	0.44	0	1
4	0.39	0.22	0	0.77	0.71	0.19	0	1	0.60	0.34	0	1
5	0	0	0	0	0	0	0	0	0.05	0.07	0	0.96
6	0	0	0	0	0	0	0	0	0.96	0.07	0.10	1

Table 3-7 – Simulation grid statistics by zone for gas hydrate saturation using Archie's and AIM methods and net sand. Sh averages in Zones 1, 3 and 4 are net pore volume weighted. Net sand averages are bulk rock volume weighted.

References Cited

Collett, Timothy S., 1993, Natural gas hydrates of the Prudhoe Bay and Kuparuk River ares, North Slope, Alaska: American Association of Petroleum Geologists Bulletin, v. 77, no. 5, pp 793-812

Mailloux, Jason, 2009, "Appendix C: Petrophysical Evaluation of Potential Hydrate-Bearing Wells on the North Slope of Alaska," *in* Schoderbek, David, Progress Report, Second Quarter 2009, ConocoPhillips Gas Hydrate Production Test (DOE Award No.: DE-NT0006553)

National Energy Technology Laboratory

626 Cochrans Mill Road
P.O. Box 10940
Pittsburgh, PA 15236-0940

3610 Collins Ferry Road
P.O. Box 880
Morgantown, WV 26507-0880

13131 Dairy Ashford, Suite 225
Sugarland, TX 77478

1450 Queen Avenue SW
Albany, OR 97321-2198

2175 University Ave. South
Suite 201
Fairbanks, AK 99709

Visit the NETL website at:
www.netl.doe.gov

Customer Service:
1-800-553-7681